MINISTRY OF HEALTH

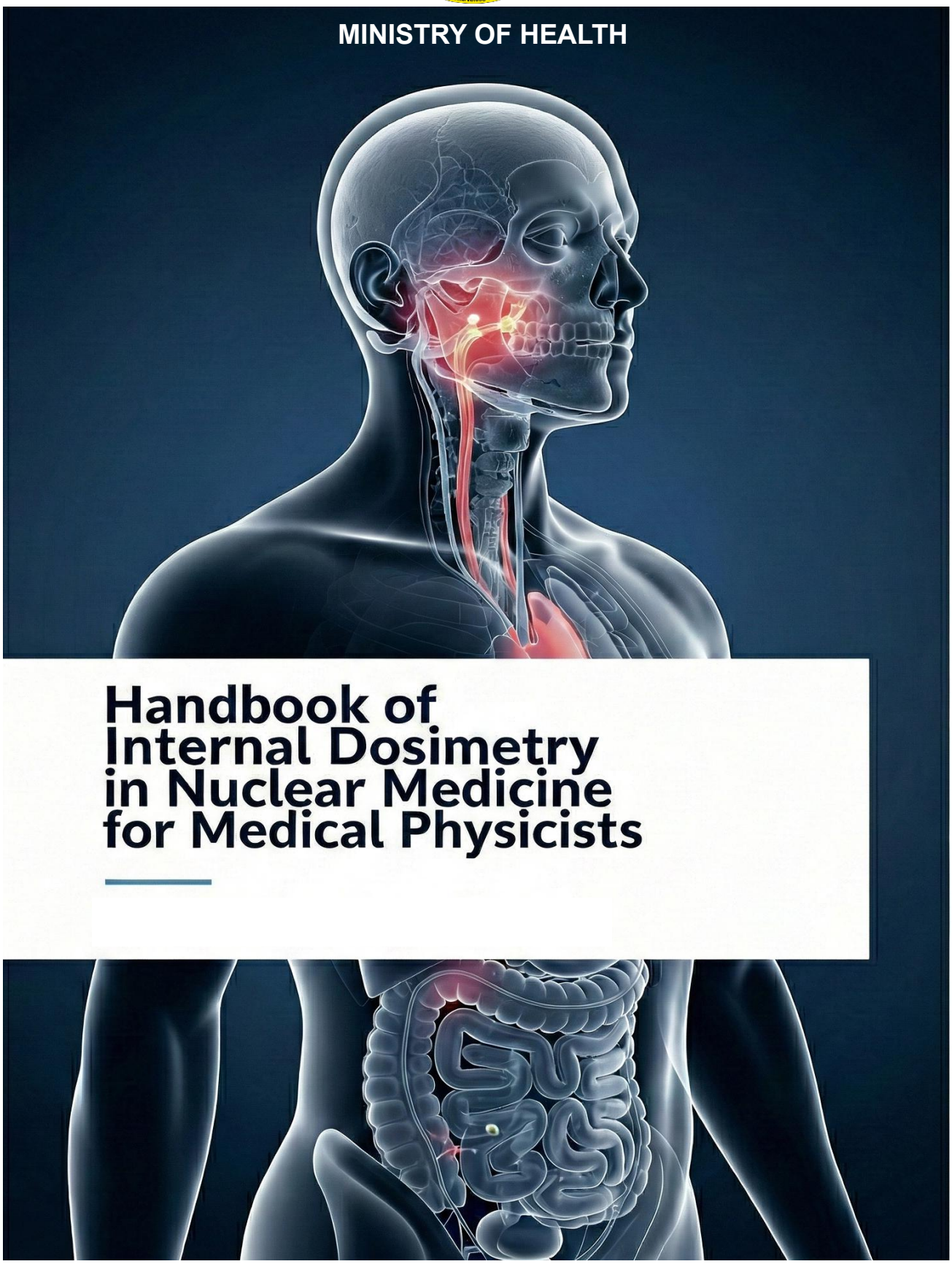

Handbook of Internal Dosimetry in Nuclear Medicine for Medical Physicists

MEDICAL RADIATION SURVEILLANCE DIVISION
2026

HANDBOOK OF INTERNAL DOSIMETRY

IN NUCLEAR MEDICINE

FOR MEDICAL PHYSICISTS

MINISTRY OF HEALTH
MEDICAL RADIATION SURVEILLANCE DIVISION
2026

Year 2026

Published by:

Ministry of Health Malaysia
Medical Radiation Surveillance Division
Level 3 & 4, Block E3, Complex E, Precinct 1
Federal Government Administrative Centre
62590 Putrajaya Malaysia
Tel : +603-88924727
Email : bkrp@moh.gov.my

Data Pengkatalogan-dalam-Penerbitan

Perpustakaan Negara Malaysia

Rekod katalog untuk buku ini boleh didapati dari Perpustakaan Negara Malaysia

eISBN 978-967-2469-87-2

FOREWORD

It gives me great pleasure to present the *Handbook of Internal Dosimetry in Nuclear Medicine for Medical Physicists*, developed by the Medical Radiation Surveillance Division, Ministry of Health Malaysia.

Nuclear medicine is an integral component of modern healthcare, providing invaluable diagnostic and therapeutic services to patients. As the field continues to advance, ensuring patient safety and the effectiveness of procedures remains a top priority. Internal dosimetry, which quantifies the radiation absorbed by patients, is a crucial element in safeguarding quality, optimizing treatment outcomes, and adhering to international standards of radiation protection.

This handbook has been developed as a comprehensive reference for medical physicists working in both government and private healthcare facilities. It consolidates fundamental principles, standardized methodologies, and practical guidance for internal dosimetry practice in nuclear medicine. By providing this resource, the Ministry of Health aims to strengthen the consistency and accuracy of dosimetry practices across the country, thereby enhancing patient care and professional competency.

I would like to commend the dedicated team of experts, especially medical physicists who contributed their knowledge, expertise, and commitment towards the development of this handbook. It is my hope that this publication will serve as a trusted reference for medical physicists and related professionals, and will continue to support the safe, effective, and sustainable advancement of nuclear medicine services in Malaysia.

Datuk Dr. Mahathar bin Abd Wahab
Director General of Health
Ministry of Health Malaysia

PREFACE

The practice of internal dosimetry is fundamental to nuclear medicine, where accurate estimation of absorbed radiation dose is critical for both diagnostic and therapeutic applications. With the increasing complexity of radiopharmaceuticals and treatment protocols, medical physicists are required to apply standardized, precise, and reproducible methods in order to ensure patient safety and optimize clinical outcomes.

This *Handbook of Internal Dosimetry in Nuclear Medicine for Medical Physicists* has been developed to provide a structured reference for physicists working in facilities that deliver nuclear medicine services, both in the public and private sectors. The content covers fundamental principles of internal dosimetry, step-by-step methodologies, calculation models, and case-based applications relevant to the Malaysian healthcare setting.

The objective of this handbook is to support harmonization of dosimetry practices across institutions, in line with international recommendations and local regulatory requirements. It is intended to be used as a day-to-day reference for physicists, complementing existing guidelines and serving as a practical resource for routine quality assurance, dose optimization, and research.

This publication is the result of collaborative efforts by all public medical physicists in the nation. Their contributions have ensured that the handbook is both scientifically robust and practically applicable to the Malaysian context.

It is my hope that this handbook will strengthen the capacity of medical physicists to carry out their professional duties with greater accuracy and confidence, ultimately contributing to the advancement of nuclear medicine services in Malaysia.

Bazli bin Sapiin
Director
Medical Radiation Surveillance Division
Ministry of Health Malaysia

ACKNOWLEDGEMENT

The preparation of the *Handbook of Internal Dosimetry in Nuclear Medicine for Medical Physicists* represents a significant step forward in strengthening internal dosimetry practice in Malaysia. This handbook provides a structured national reference to support the safe, accurate, and consistent implementation of dosimetry procedures across nuclear medicine facilities in both the public and private sectors.

As medical physicists serving under the Ministry of Health Malaysia, we are honored to contribute to this important initiative. We express our sincere appreciation to the Ministry, particularly the Medical Radiation Surveillance Division, for the trust and opportunity to share our professional knowledge and clinical experience in the development of this handbook. This effort reflects the Ministry's strong commitment to advancing medical physics practice and enhancing the quality of patient care.

We extend special gratitude to our colleagues, clinicians, and technical experts who provided valuable input and constructive feedback throughout the development process. Their expertise ensured that the content remains scientifically accurate, clinically relevant, and aligned with the practical needs of the Malaysian healthcare system. We also acknowledge Dr. Mark Willem Konijnenberg, Physicist and Radiation Protection Officer at the Department of Radiology and Nuclear Medicine, Erasmus MC, and Dr. Jens Kurth, Head of Medical Physics at the Department of Nuclear Medicine, Rostock University Medical Center, Germany, for their expert insights and scientific discussions. Their contributions strengthened the interpretation of dosimetric principles and improved the methodological rigor of this handbook.

We hope this handbook will serve as a reliable resource for medical physicists and other professionals involved in nuclear medicine. We aim for it to promote standardized practice, support continuous professional development, and contribute to the sustainable growth of nuclear medicine services nationwide

.

TABLE OF CONTENT

DEFINITIONS

Term	Definition
Absorbed Dose (AD)	Energy deposited by ionizing radiation per unit mass of tissue. Unit in Gray (Gy).
Biological Kinetics	Time-dependent behaviour of radiopharmaceutical absorption, distribution, metabolism, and excretion, considering both the radionuclide and its carrier molecule.
DOTATATE	Radiolabeled somatostatin analog used for imaging and therapy of neuroendocrine tumors.
Effective Dose	Risk-related dose quantity that accounts for absorbed dose, radiation type, and tissue weighting factors to estimate stochastic health risk.
Gray (Gy)	SI unit of absorbed dose, equal to one joule per kilogram.
Internal Dosimetry	Measurement and assessment of absorbed dose delivered to tissues and organs following the intake of radionuclides.
Linear Energy Transfer (LET)	Mean energy deposited by a charged particle per unit path length. Units in J m^{-1} or commonly keV μm^{-1}.
Metastatic Castration-Resistant Prostate Cancer (mCRPC)	Advanced prostate cancer that progresses despite androgen deprivation therapy.
Monte Carlo (MC)	Stochastic simulation method is used to model radiation transport and energy deposition.
Neuroendocrine Tumor (NET)	Tumor originating from neuroendocrine cells, commonly expressing somatostatin receptors.
Number of Disintegrations	Total number of nuclear decay events occurring in a source region over time, also termed time-integrated activity or cumulated activity.
Prostate-Specific Antigen (PSA)	Serum biomarker is used for diagnosis, staging, and monitoring of prostate cancer.

Prostate-Specific Membrane Antigen (PSMA)	Transmembrane protein overexpressed in prostate cancer cells and targeted in radioligand therapy.
S-value	Mean absorbed dose to a target region per unit time-integrated activity in a source region.
Selective Internal Radiation Therapy (SIRT)	Intra-arterial radionuclide therapy using microspheres, primarily for liver malignancies.
Somatostatin Receptor (SSTR)	Cell-surface receptor overexpressed in many neuroendocrine tumors and targeted in radionuclide therapy.
Source Organ	Organ or tissue in which the radiopharmaceutical localizes and emits radiation.
Specific Absorbed Fraction (SAF)	Fraction of emitted energy absorbed in a specified target region per unit mass of that region.
Target Organ	Organ or tissue receiving radiation energy, often referring to healthy organs at risk during molecular radionuclide therapy.
Tumor Absorbed Dose	Radiation energy absorbed per unit mass of tumor tissue, used to evaluate therapeutic effectiveness in radiopharmaceutical therapy.

ABBREVIATIONS

Ã	Time-Integrated Activity
ADME	Absorption, Distribution, Metabolism, and Excretion
AHASA	As High As Safely Administrable
ALARA	As Low As Reasonably Achievable
BED	Biological Effective Dose
CT	Computed Tomography
DNA	Deoxyribonucleic Acid
DOTATATE	DOTA-0-Tyr^3-Octreotate
DPK	Dose Point Kernel
DTC	Differentiated Thyroid Carcinoma
DTPA	Diethylenetriaminepentaacetic Acid
DVH	Dose Volume Histogram
EANM	European Association of Nuclear Medicine
EMA	European Medicines Agency
FDA	Food and Drug Administration
FDG	Fluoro-2-Deoxy-D-Glucose
GLUT	Glucose Transporters
HDP	Hydroxy Methylene Diphosphonate
IAEA	International Atomic Energy Agency
ICRP	International Commission on Radiological Protection
IV	Intravenous
LET	Linear Energy Transfer
MAA	Macroaggregated Albumin

MC	Monte Carlo
MDP	Methylene Diphosphonate
mCRPC	Metastatic Castration-Resistant Prostate Cancer
MIBG	Metaiodobenzylguanidine
MIRD	Medical Internal Radiation Dose
MRT	Molecular Radiotherapy
NaF	Sodium Fluoride
NaI	Sodium Iodide
NET	Neuroendocrine Tumor
NTCP	Normal Tissue Complication Probability
NURBS	Non-Uniform Rational B-Splines
OAR	Organ at Risk
OLINDA	Organ Level Internal Dose Assessment
ORNL	Oak Ridge National Laboratory
PET	Positron Emission Tomography
PET/CT	Positron Emission Tomography and Computed Tomography
PRRT	Peptide Receptor Radionuclide Therapy
PSMA	Prostate-Specific Membrane Antigen
PVC	Partial Volume Correction
PVE	Partial Volume Effect
QUANUM	Quality Management Audits in Nuclear Medicine
RES	Reticuloendothelial System
ROI	Region of Interest
SIRT	Selective Internal Radiation Therapy

SPECT	Single Photon Emission Computed Tomography
SPECT/CT	Single Photon Emission Computed Tomography and Computed Tomography
SSTR	Somatostatin Receptor
SUV	Standard Uptake Value
TCP	Tumor Control Probability
VOI	Volume of Interest
WB	Whole Body

CHAPTER 1

INTRODUCTION

Internal dosimetry is the science of estimating and assessing the radiation dose received by tissues and organs within the body from radionuclide substances that have been ingested, injected, inhaled, or absorbed through the skin. It involves evaluating the amount, spatial distribution, and temporal distribution of radiation energy deposited in tissues by radionuclides within the body. This field is crucial for assessing health risks associated with internal contamination and ensuring the safety of individuals working with or exposed to radionuclide materials.

1.1 Importance of Internal Dosimetry in Medicine

In medicine, internal dosimetry plays a key role in assessing the radiation doses absorbed by tissues and organs following the administration of radiopharmaceuticals. It is particularly essential in nuclear medicine therapies involving radionuclides such as Iodine 131 (I-131), Lutetium 177 (Lu-177), Yttrium 90 (Y-90) and others. In line with the principle of As High As Safely Administrable (AHASA), internal dosimetry enables personalized treatment planning and allows for the optimization of therapeutic radiopharmaceutical doses by maximizing tumor irradiation while ensuring safe limits for normal organs are not exceeded. This allows clinicians to maximize therapeutic efficacy by delivering optimal doses to target lesions. It also minimizes toxicity by avoiding excessive exposure to healthy tissues, ensures patient safety and comply with regulatory requirements. With increasing use of molecular radiotherapy (MRT) and theranostic, internal dosimetry is becoming a foundation of precision medicine in oncology and beyond.

1.2 Therapeutic Applications of Internal Dosimetry

When radionuclides are incorporated into target tissue-avid radiopharmaceuticals in sufficient amounts, they can deliver a high absorbed dose (AD) to produce a therapeutic response in tumors or other target tissues. As administered activities and normal tissue absorbed doses increase, the risk of serious radiation injury also rises. Therefore, it is crucial to establish absorbed doses for both target and normal tissues with reasonable accuracy and precision, utilizing reliable dose-response relationships for target tissues and dose-toxicity relationships for normal tissues.

1.3 Advances in Radiation Dosimetry in Nuclear Medicine

The growth of targeted radionuclide therapies is driving a paradigm shift in internal dosimetry. The field is transitioning from generalized organ-average calculations toward personalized, voxel-level estimations tailored to individual patients.

1) **Patient-specific dosimetry**: This method estimates the radiation dose to tissues of a specific patient based on their individual body habitus and measured radiopharmaceutical kinetics rather than using an average anthropomorphic model and hypothetical kinetics or patient cohort avaraged kinetics.

2) **Position-specific dosimetry**: Unlike standard models that assume an "average" dose across a target, position-specific dosimetry maps the actual energy delivered to specific points or voxels. This allows for a more accurate assessment of "hot" and "cold" spots within a tumor or organ, reflecting the reality that radiation is rarely distributed evenly.

1.4 Key Elements in Internal Dosimetry

There are several key elements in internal dosimetry:

1) **Radionuclide Intake**: Determining how radionuclide substances enter the body, whether through inhalation, ingestion, absorption or injection (either intravenous or intra-arterial).

2) **Biokinetics**: Understanding how these radionuclides are distributed, metabolized and eliminated within the body. This involves studying the rates of uptake and clearance from different organs and tissues.

3) **Dosimetric Models**: Developing mathematical models to estimate the distribution of radionuclides within the body and to calculate the radiation dose delivered to specific organs and tissues.

4) **Absorbed Dose Calculation**: Using dosimetric models to compute the AD, which is the amount of energy deposited by radiation per unit mass of tissue and the equivalent dose, which accounts for the biological effectiveness of different types of radiation.

5) **Bioassay and Monitoring**: Techniques for measuring the amount of radionuclide material in the body or in biological samples (like urine or blood) to assess AD.

6) **Risk Assessment**: Assessing the biological risks associated with AD, specifically regarding stochastic effects like carcinogenesis and deterministic tissue reactions such as acute organ damage.

7) **Toxicity**: Toxicity generally refers to the adverse biological effects caused by radiopharmaceuticals, which are drugs that contain radionuclide isotopes used for diagnosis or therapy. Toxicity can arise from radiation exposure, the chemical properties of the compound or both. Diagnostic nuclear medicine generally involves low radiation doses, making toxicity rare. Therapeutic applications involve higher doses, requiring dosimetry and monitoring to manage toxicity.

1.5 References

Bolch, W. E., Bouchet, L. G., Robertson, J. S., Wessels, B. W., Siegel, J. A., Howell, R. W., Erdi, A. K., Aydogan, B., Costes, S., Watson, E. E., & others. (2009). MIRD pamphlet no. 21: A generalized schema for radiopharmaceutical dosimetry—Standardization of nomenclature. *Journal of Nuclear Medicine, 50*(3), 477–484.

Stabin, M. G. (2006). Fundamentals of internal dosimetry in nuclear medicine. *Seminars in Nuclear Medicine, 36*(2), 102–114.

Stabin, M. G. (2008). *Radiation protection and dosimetry: An introduction to health physics.* Springer.

CHAPTER 2

RADIATION INTERACTION AND DOSIMETRY QUANTITY

The principles of radiation interaction and dosimetric quantities are essential for analyzing the impact of radiation on matter, particularly biological tissue. As ionizing radiation traverses a medium, it deposits energy through atomic ionization and excitation, establishing the physical basis for dose measurement. By utilizing specific dosimetric quantities, we can quantify energy deposition and predict biological responses, which is critical for maintaining safety standards in clinical environments.

2.1 Radiation Interaction with Tissue

Charge particles and photons, especially gamma rays, play a pivotal role both in delivering AD to tissues and enabling imaging for quantification. Understanding the nature of photon tissue interactions is essential to model radiation transport, estimate AD, and improve image-based dosimetry methods such as voxel level SPECT/PET dosimetry. Three main interactions and mechanisms of photons and charged particles relevant to nuclear medicine include the photoelectric effect, Compton scattering, and pair production for photons, and alpha particles, beta particles, and Auger electrons for charged particles.

Dosimetric quantities such as AD, equivalent dose (H_T), and effective dose (ED) are fundamental to internal dosimetry, as they provide a standardized framework to quantify radiation exposure, assess biological effects, and ensure safe and effective use of radiopharmaceuticals in diagnostic and therapeutic nuclear medicine

2.1.1 Photoelectric Effect

The energy range for photoelectric effect is dominant for low-energy photons (typically <100 keV). A photon interacts with a tightly bound inner-shell electron (usually K or L shell) as shown in Figure 2.1. The photon is completely absorbed, and the electron is ejected with kinetic energy equal to:

$$E_e = E_y - E_b \qquad \text{Equation 2-1}$$

Where E_y is the photon energy and E_b is the binding energy of the electron.

The vacancy in the electron shell leads to characteristic X-ray emission or Auger electron cascade.

The probability of photoelectric interaction is highly dependent on the atomic number of absorbing materials. Hence, bone with high atomic number shows more photoelectric absorption than soft tissue with low atomic number. In terms of dosimetry relevance, local dose deposition of photoelectric effect due to complete energy absorption.

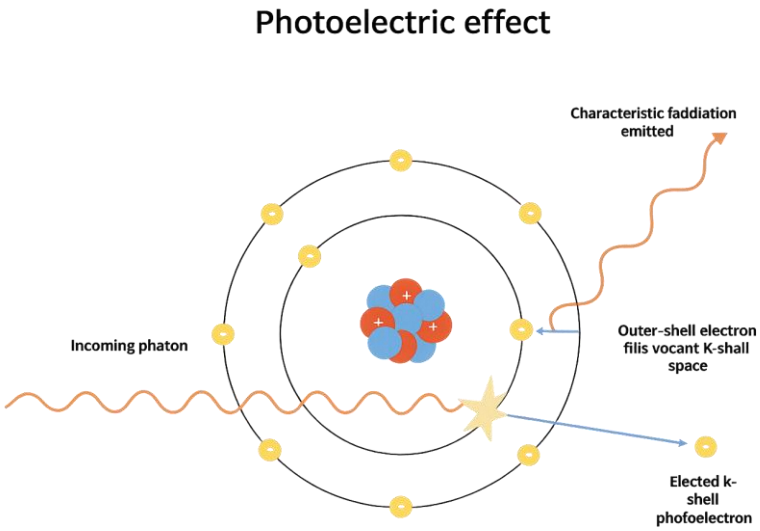

Figure 2.1: Illustration of the photoelectric effect showing the interaction of an incoming photon with an inner-shell electron. The photon transfers all its energy to the electron, ejecting it from the atom as a photoelectron. The resulting electron vacancy is filled by an outer-shell electron, releasing characteristic X-rays in the process.

2.1.2 Compton Scattering

The energy range for Compton scattering dominates in the energy range of most nuclear medicine radionuclides (100 keV – 10 MeV). For Compton scattering examples mostly occurred in Lu-177 (208 keV), I-131 (364 keV) and Y-90 Bremsstrahlung (up to ~2.3 MeV). A photon collides with a loosely bound or free outer-shell electron as shown in Figure 2.2. The photon is scattered at an angle θ and loses part of its energy to the electron, which is ejected:

$$E'_{\gamma}=1+\frac{E_{\gamma}}{1+\frac{E_{\gamma}}{m_e c^2}(1-\cos\theta)} \qquad \text{Equation 2-2}$$

Where E'_{γ} is the scattered photon energy and $m_e c^2$ is the rest mass energy of the electron (~511 keV).

Compton scattering is dependent on atomic number and proportional to electron density, which is similar across most soft tissues. Hence, uniform across organs,

contributing to widespread background dose. In terms of dosimetry relevance, partial energy deposition leads to scatter dose outside the target volume.

The clinical impact of this interaction gives a major contribution to systemic dose in MRT (e.g., in whole body dosimetry for I-131 thyroid ablation), and important consideration in organ at risk dose estimation, especially for kidneys, bone marrow, and lungs.

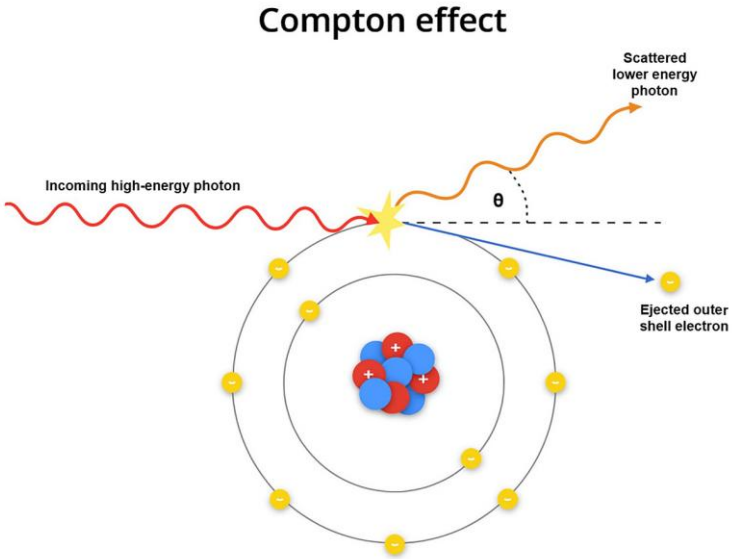

Figure 2.2: Diagram illustrating the Compton effect, where an incoming high-energy photon collides with a loosely bound outer-shell electron. The photon transfers part of its energy to the electron, ejecting it from the atom, while the photon itself is scattered at an angle (θ) with reduced energy. This interaction dominates in the intermediate energy range commonly encountered in diagnostic nuclear medicine.

2.1.3 Pair Production

The energy threshold of pair production occurs only when photon energy is more than 1.022 MeV (twice the rest mass of the electron, 511 keV × 2). The photon interacts with the electric field of the nucleus, and its energy is converted into a matter antimatter pair

$$A_{\gamma} = e^{-} + e^{+} \qquad \text{Equation 2-3}$$

The positron (e^{+}) quickly annihilates with an electron, releasing two 511 keV photons at 180° of positron emission tomography (PET) imaging. Probability increases with atomic number and photon energy above the threshold.

Hence, the dosimetric relevance for this type of interaction is not significant in low to mid energy radionuclides used in single photon emission computed

tomography (SPECT). Annihilation is crucial in positron emitters such as F-18, Ga-68 and I-124. The annihilation photons are detected for image reconstruction but do not deposit dose at the annihilation site (non-local energy deposition). In therapeutic PET radionuclides such as Cu-64 and Zr-89, positrons undergo annihilation after decay, while pair production remains negligible because the 1.346 MeV photon of Cu-64 yields only a low interaction probability and the 909 keV gamma ray of Zr-89 lies below the pair-production threshold, yet this small component still influences image-based dosimetry that you derive from PET data.

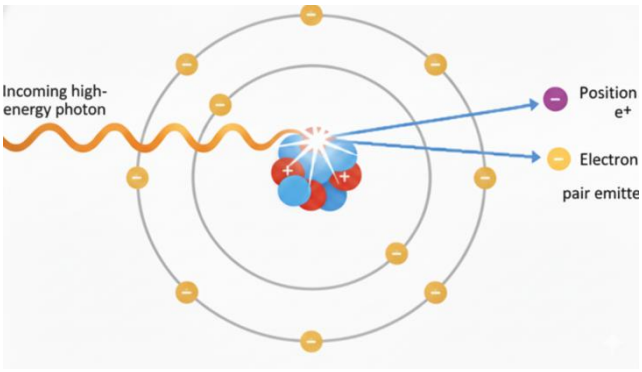

Figure 2.3: Illustration of pair production, a high-energy photon interaction that occurs when photon energy exceeds 1.022 MeV. The photon interacts with the nuclear field, converting its energy into a particle antiparticle pair an electron and a positron. The positron eventually annihilates with an electron, producing two 511 keV annihilation photons emitted in opposite directions.

2.2 Charged Particle Interactions

Charged particles including beta particles, alpha particles, and Auger electrons are critically important in internal dosimetry due to their capacity to deposit energy directly along their short-range paths, causing localized biological damage.

2.2.1 Alpha

Alpha particles emitted by radionuclides like Actinium 225 (Ac-225) have a very short path length (~50–100 μm) but exhibit high Linear Energy Transfer (LET), making them highly cytotoxic within a confined range.

Due to their short path, even minor mis-localization can lead to underdosing the target or damaging normal cells, although precise biodistribution is essential to avoid off-target toxicity due to their potent biological effects.

2.2.2 Beta

Beta particles, such as those emitted by Lu-177, Y-90, and I-131, possess a medium range in tissue (typically a few millimeters) and primarily induce ionization and excitation as they traverse through tissue.

Deposition of the absorbed dose over a larger volume than just at cellular scale will allow for crossfire effect, beneficial in tumors with non-uniform uptake.

These particles play a direct role in therapeutic dose delivery and are commonly modeled using dose point kernels (DPK) or Monte Carlo (MC) simulations for accurate absorbed dose calculations.

2.2.3 Auger Electrons

Auger electrons released during electron transitions (e.g., from Iodine 123 (I-123), Terbium 161(Tb-161), exhibit an ultra-short range (in the nanometer to micrometer scale). Localized dose delivery due to their short range, Auger electrons can deliver a high radiation dose to DNA if the radiopharmaceutical is internalized into the nucleus. Selective cytotoxicity ideal for targeting single cells, micro metastases, or minimal residual disease, provided precise subcellular localization is achieved.

The interactions of these three charged particles with biological tissue are summarized in Table 2.1.

Table 2.1: Summary table of charge particles interaction with tissue.

Particle Type	Range in Tissue	LET (Energy Deposition)	Dosimetric Impact	Modeling Approach
Beta	Millimeter scale	(~0.2 keV/μm)	organ AD	Medical Internal Radiation Dose (MIRD) formalism using S-values or dose factors.
Alpha	Micrometer scale	(~100 keV/μm)	Microscopic energy deposition analysis	Micro dosimetry
Auger Electrons	Nanometer scale	(4-25 keV/μm)	Localization at molecular or DNA scale	Cellular and subcellular dosimetry

As a conclusion, photon and charge particles interaction with tissue is very important for consideration in internal dosimetry calculation. It depends on their characteristics and dosimetry relevance of selected radiopharmaceuticals. Each radiopharmaceutical agent emits different types of radiation (beta, gamma, alpha

or auger electron), influencing their application in therapy or imaging and determining the strategies required for accurate dose estimation and monitoring.

2.3 Dosimetric Quantities

Dosimetric quantities form the foundation of radiation protection and internal dosimetry. They describe how energy from ionizing radiation is deposited in matter, the biological significance of that energy, and how overall risk is assessed. Each quantity serves a distinct purpose in quantifying exposure and biological effect.

2.3.1 Absorbed Dose (AD)

AD measures how much ionizing radiation energy is deposited in body tissues. It is expressed in grays (Gy)

$$AD = \frac{\text{energy (J)}}{\text{mass (kg)}} \qquad \text{Equation 2-4}$$

AD is particularly crucial for assessing deterministic effects such as organ toxicity and tissue damage and is central to planning both diagnostic and therapeutic procedures. For internal dosimetry, the AD is estimated by tracking how a radiopharmaceutical distributes, accumulates, and clears from the body.

2.3.2 Equivalent Dose (H_T)

The H_T is a dosimetric quantity used to assess the biological effect of ionizing radiation in specific organs or tissues. The equivalent dose accounts for the radiation type using a radiation weighting factor (W_R) to reflect biological effectiveness. The equivalent dose is expressed in sieverts (Sv) and is calculated as:

$$H_T = \sum D_{T,R} \times W_R \qquad \text{Equation 2-5}$$

Where $D_{T,R}$ define as the mean tissue or organ dose delivered by type R radiation and W_R is a radiation weighting factor.

Radiation Weighting Factors (W_R)

A dimensionless factor used to account for the relative biological effectiveness of different types of radiation when calculating the equivalent dose. It reflects the fact that different types of radiation cause different levels of biological damage for the same amount of absorbed energy.

Table 2.2: Radiation weighting factors W_R.

Radiation Type	Typical W_R Value	Notes
Photons (X-rays, gamma rays)	1	Common in diagnostic nuclear medicine; equivalent dose numerically equals AD.
Electrons (beta particles, positrons, muons)	1	Common in diagnostic and therapeutic nuclear medicine; equivalent dose numerically equals AD.
Alpha Particles	20	High biological damage: 1 Gy of alpha radiation is equivalent to 20 Gy of photon radiation in terms of biological effectiveness.
Neutrons	5 to 20+ (energy-dependent)	Values vary significantly based on neutron energy, reflecting diverse biological effects.

2.3.3 Effective Dose (ED)

ED allows for a comprehensive assessment of overall radiation risk, integrating both the type of radiation and the radiosensitivity of exposed tissues. It is calculated by summing the equivalent dose (H_T) to each tissue, multiplied by its specific tissue weighting factor (w_T), and is expressed in Sv. The value is measured is determined by the following formula:

$$ED = \sum_T W_T \times H_T \qquad \text{Equation 2-6}$$

Where W_T is the tissue weighting factor and H_T is the equivalent dose in tissue T.

Table 2.3: Tissue weighting factors according to International Commission on Radiological Protection (adapted from ICRP 103).

Tissue	W_T	ΣW_T
Bone marrow (red), Colon, Lung, Stomach, Breast and Remainder tissues*	0.12	0.72
Gonads	0.08	0.08
Bladder, Esophagus, Liver and Thyroid	0.04	0.16
Bone surface, Brain, Salivary glands and Skin	0.01	0.04
Total		1.00

*Remainder tissues: Adrenals, Extrathoracic (ET) region, Gall bladder, Heart, Kidneys, Lymphatic nodes, Muscle, Oral mucosa, Pancreas, Prostate, Small intestine, Spleen, Thymus, Uterus/cervix.

2.3.4 Linear Energy Transfer (LET)

Linear Energy Transfer (LET) is a measure of energy deposited by ionizing radiation per unit distance as it travels through a matter. It's a key concept in understanding how different types of radiation interact with matter, particularly in biological systems, and is expressed in units like keV μm^{-1} or MeV cm^{-1}. High LET radiation, such as alpha particles and neutrons, deposits energy more densely and over shorter distances, while low LET radiation, like X-rays and gamma rays, deposits energy more sparsely over longer paths.

The LET is expressed as:

$$LET = \frac{dE}{dx} \qquad \text{Equation 2-7}$$

Where *dE* is the energy deposited by a charge particle and *dx* is the distance its travel through a material.

2.4 References

Bolch, W. E., Bouchet, L. G., Robertson, J. S., Wessels, B. W., Siegel, J. A., Howell, R. W., Erdi, A. K., Aydogan, B., Costes, S., Watson, E. E., & others. (2009). MIRD pamphlet no. 21: A generalized schema for radiopharmaceutical dosimetry. *Journal of Nuclear Medicine, 50*(3), 477–484.

Eckerman, K. F., & Ryman, J. C. (1993). *External exposure to radionuclides in air, water, and soil.* Oak Ridge National Laboratory.

Hall, E. J., & Giaccia, A. J. (2012). *Radiobiology for the radiologist* (7th ed.). Lippincott Williams & Wilkins.

International Commission on Radiological Protection (ICRP). (1979). *Limits for intakes of radionuclides by workers, Part 1* (ICRP Publication 30).

Kassis, A. I. (2011). Molecular and cellular radiobiological effects of Auger emitting radionuclides. *Radiation Protection Dosimetry, 143*(2–4), 241–247.

International Commission on Radiological Protection (ICRP). (1991). *1990 recommendations of the International Commission on Radiological Protection* (ICRP Publication 60). *Annals of the ICRP, 21*(1–3).

International Commission on Radiological Protection (ICRP). (2007). *The 2007 recommendations of the International Commission on Radiological Protection* (ICRP Publication 103). *Annals of the ICRP, 37*(2–4).

Kangasmaa, T. S., Constable, C., & Sohlberg, A. O. (2018). Evaluation of quantitative 123I and 131I SPECT with Monte Carlo-based down-scatter compensation. *Nuclear Medicine Communications, 39*(12), 1097–1102.

Kim, M., Bae, J. K., Hong, B. H., Kim, K. M., & Lee, W. (2019). Effects of collimator on imaging performance of yttrium-90 bremsstrahlung photons: Monte Carlo simulation. *Nuclear Engineering and Technology, 51*(2), 539–545.

Martin, A., & Harbison, S. (2018). *An introduction to radiation protection* (7th ed.). CRC Press.

Noori-Asl, M., & Bitarafan-Rajabi, A. (2019). Simulation and patient studies of scatter correction in cardiac SPECT imaging. *Iranian Journal of Medical Physics, 16*(6), 430–438.

Porter, C. A., Bradley, K. M., Hippeläinen, E. T., Walker, M. D., & McGowan, D. R. (2018). Phantom and clinical evaluation of the effect of full Monte Carlo collimator modelling in post-SIRT yttrium-90 bremsstrahlung SPECT imaging. *EJNMMI Research, 8*, 36.

Shahmari, N., & Taherparvar, P. (2019). Evaluation of the effect of different collimators and energy window on Y-90 bremsstrahlung SPECT imaging by SIMIND Monte Carlo program. *Nuclear Medicine Review, 22*(2), 45–55.

Stabin, M. G. (2008). *Fundamentals of nuclear medicine dosimetry.* Springer.

Xiang, H., Lim, H., Fessler, J. A., & Dewaraja, Y. K. (2019). SPECT/CT scatter estimation using a deep convolutional neural network: Implementation in Y-90 imaging. In *2019 IEEE Nuclear Science Symposium and Medical Imaging Conference (NSS/MIC).*

CHAPTER 3

RADIOPHARMACEUTICAL AND BIOLOGICAL PHARMACOKINETIC

Radiopharmaceuticals are compounds developed for use in nuclear medicine to support diagnostic imaging and therapeutic procedures. Each consists of a radionuclide isotope linked to a molecule that targets specific biological pathways within the body. The radionuclide provides the measurable signal or therapeutic effect, while the overall performance and safety depend on both the pharmacokinetics of the compound and the physical and chemical properties of the radionuclide itself.

3.1 Radionuclide Properties in Nuclear Medicine

Radionuclides in nuclear medicine are chosen based on physical and radiological properties that match clinical goals, either for diagnostic imaging or therapy. Diagnostic radionuclides emit gamma rays or positrons detectable by imaging devices, while therapeutic ones emit beta or alpha particles for targeted cell destruction.

Key selection criteria include:

1) **Half-life**: Should align with the biological kinetics of the tracer and clinical procedure schedule.

2) **Type and energy of emission**: Gamma and positron emitters are used for imaging; beta and alpha emitters for therapy.

3) **Production method**: Determines availability and cost (e.g., reactor, generator or cyclotron).

The careful selection of radionuclides ensures optimal performance in clinical applications, balancing absorbed dose, image quality, and biological compatibility. Table 3.1 summarizes the commonly used radionuclides for these applications.

Table 3.1: Key properties of radionuclides frequently used in MRT dosimetry.

Radionuclide	Half-life	Mean Energy (MeV)	Emission Type	Common Clinical Applications
I-131	~8.02 days	Beta: 0.606	Beta & Gamma	sodium iodide for therapy of differentiated thyroid cancer
Y-90	~64.1 hours	Beta: 0.934	Beta Only	use microspheres for liver cance therapy
Lu-177	~6.65 days	Beta: 0.133	Beta & Gamma	use DOTATATE for neuroendocrine tumors and PSMA for prostate cancer

3.2 Biological Kinetics of Radiopharmaceutical

Radiopharmaceuticals are key to nuclear medicine, used for both imaging and therapy. They are made up of two main parts:

1) **Radionuclide** – the radionuclide element that emits radiation for detection or treatment.

2) **Carrier (ligand) molecule** – a compound (like a peptide or antibody) that directs the radionuclide to specific organs or tissues in the body.

Often, a chelator (such as DOTA) is added to bind the radionuclide securely to the carrier (Figure 3.1). A good radiopharmaceutical must be stable in the body, stay targeted to the correct area, and avoid harming healthy tissues. It should also work well with imaging system or therapy applications.

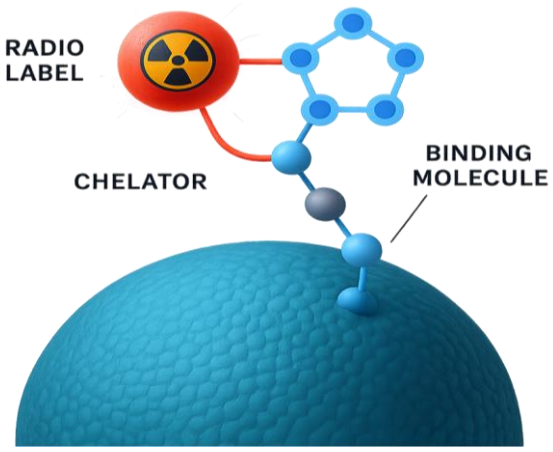

Figure 3.1: Structure of a radiopharmaceutical agent with chelator.

Understanding biological kinetics on how the radiopharmaceutical move through the body is equally important. This includes how it's absorbed, distributed, metabolized, and excreted (ADME) as illustrated in Figure 3.2. These factors affect how well it targets specific tissues and help determine how much radiation

each organ receives. Accurate knowledge of biological kinetics is essential for nuclear medicine dosimetry, which is the calculation of radiation dose. It ensures safe and effective therapy tailored to each patient.

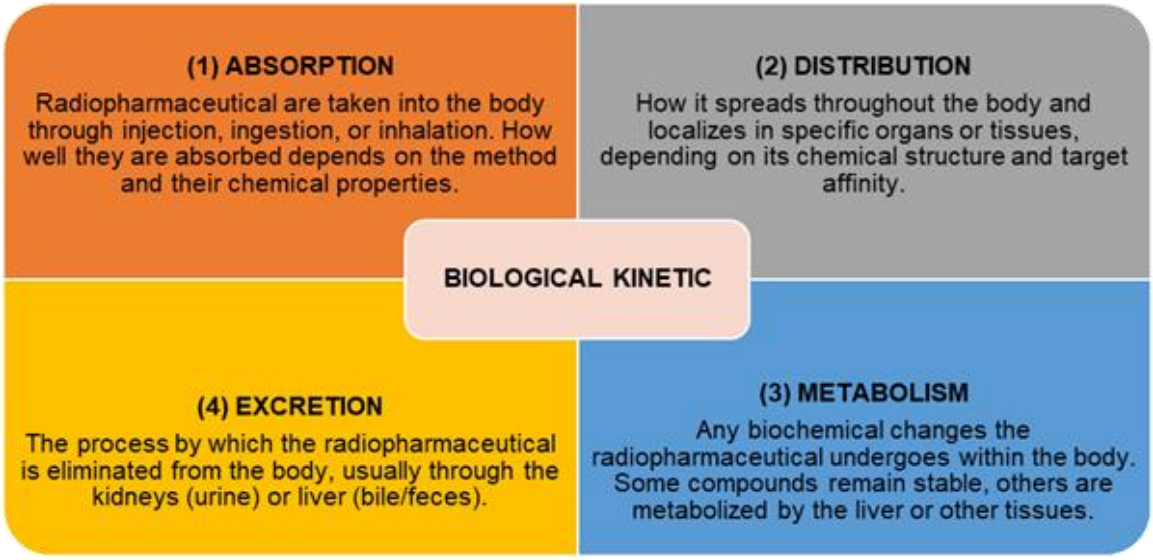

Figure 3.2: Biological kinetics of radiopharmaceuticals: ADME Overview.

Table 3.2 outlines the ADME characteristics of radionuclides frequently employed in therapeutic nuclear medicine, such as I-131, Y-90, and Lu-177, while Table 3.3 describes those of diagnostic radionuclides like Tc-99m and F-18, providing a comparative view that highlights their biological behavior and informs appropriate clinical selection.

Table 3.2*:* Absorption, Distribution, Metabolism, and Excretion (ADME) of MRT.

Radiopharmaceutical	Absorption	Distribution	Metabolism	Excretion
I-131 Nal	Systemic	Thyroid and iodine-avid tissues	Minimal	Urine and feces
I-131 MIBG	Systemic	Adrenergic tissues and neuroendocrine tumors	Minimal	Renal
Y-90 microsphere	Local	Targeted tissue vasculature	Negligible	Radionuclide decay
Lu-177 PSMA	Local	PSMA-expressing tissues	Partial	Renal
Lu-177 DOTATATE	Systemic	SSTR2 in neuroendocrine tumors; kidneys, spleen, liver, bone marrow uptake	Minimal	Renal

Table 3.3: Absorption, Distribution, Metabolism, and Excretion (ADME) of diagnostic radionuclides.

Radiopharmaceutical	Absorption	Distribution	Metabolism	Excretion
Tc-99m MDP	Systemic	Bone and soft tissue depending on uptake	None	Renal
Tc-99m DTPA	Systemic	Extracellular fluid; no cell binding; brain, kidneys, bladder	None	Renal
Tc-99m MAA	Local	Pulmonary capillaries; minimal systemic spread	None	Renal/RES
F-18 FDG	Systemic	Metabolically active tissues	Partial (glucose analog)	Renal/hepatic
F-18 NaF	Systemic	Bone hydroxyapatite; reflects bone turnover	None	Renal

Different radiopharmaceuticals are used in nuclear medicine depending on the type of radionuclide and the clinical purpose. Each radiopharmaceutical is designed to target specific organs or tissues, using various uptake mechanisms like active transport or receptor binding.

Table 3.4 and Table 3.5 and presents examples of radiopharmaceuticals used in both therapeutic and diagnostic applications, outlining their target organs, mechanisms of action within the body, and effective half-lives.

Table 3.4: Critical organs of MRT Radiopharmaceuticals.

Radiopharmaceutical	Organ at Risk	Uptake Mechanism	Biological Half-Life	References
I-131 NaI	Thyroid	Na-I symporter; organification	~5–7 d	ICRP Publication 128
	Salivary glands	Na-I symporter; secretion	~1–2 d	Liu et al. (2011)
	Stomach wall	Active iodide secretion	~1–2 d	ICRP Publication 53
	Bladder wall	Renal filtration; excretion	~12–24 h	Brill et al. (2006)
	Remainder tissues	Systemic recirculation	~1 d	Lassmann et al. (2008)
I-131 MIBG	Tumor	norepinephrine transporter; vesicular uptake	~2–3 d	Matthay et al. (2010)
	Liver	NET-independent uptake; metabolism	~1–2 d	ICRP Publication 128

	Bone marrow	Circulating activity; nonspecific uptake	~1–2 d	Gelfand et al. (2011)
	Bladder wall	Renal clearance	~1 d	ICRP Publication 128
	Thyroid	Na-I symporter	~1–2 d	Sudbrock et al. (2010)
Y-90 microspheres	Liver parenchyma	Permanent vascular trapping	~2.67 d (physical)	Salem & Thurston (2006)
	Lungs	Capillary trapping	~2.67 d (physical)	Kao et al. (2013)
	GI tract	Non-target embolization	~2.67 d (physical)	Murthy et al. (2007)
Lu-177 PSMA	Tumor	PSMA receptor binding	~3–5 d	Sartor et al. (2021); Okamoto et al. (2017)
	Kidneys	Tubular reabsorption of PSMA ligands	~3–5 d	Okamoto et al. (2017)
	Salivary Glands	PSMA expression; secretion	~3–4 d	Klein Nulent et al. (2019)
	Lacrimal Glands	PSMA expression	~3–4 d	Okamoto et al. (2017)
	Bone Marrow	Circulating activity (Blood pool)	~1–2 d	Sartor et al. (2021)
Lu-177 DOTATATE	Tumor	SSTR2 receptor binding	~4–6 d	Strosberg et al. (2017)
	Kidneys	Proximal tubule reabsorption	~4–6 d	Sandström et al. (2013)
	Liver	SSTR expression; metabolism	~2–3 d	Garske et al. (2012)
	Spleen	SSTR2 binding; RES uptake	~2–3 d	Sandström et al. (2013)
	Bone Marrow	Blood pool activity	~1–2 d	Strosberg et al. (2017)

Table 3.5: Critical organs of diagnostic radiopharmaceuticals.

Radiopharmaceutical	Organ at Risk	Uptake Mechanism	Effective Half-Life	References
Tc-99m MDP	Bone	Chemisorption to hydroxyapatite	~6 h	ICRP 53
	Bladder wall	Renal clearance	~6 h	ICRP 53
	Soft tissue	Transient distribution	~6 h	ICRP 53
Tc-99m DTPA	Bladder wall	Glomerular filtration	~6 h	ICRP 53
	Kidneys	Renal clearance	~6 h	ICRP 53

Tc-99m MAA	Lung	Capillary trapping	~6 h (physical)	ICRP 53
	Liver/spleen	Capillary trapping	~6 h (physical)	ICRP 53
F-18 FDG	Brain	Glucose Transporters (GLUT) transport; phosphorylation	~1.5–2 h	ICRP 128; MIRD 18
	Myocardium	GLUT transport	~1.5–2 h	ICRP 128
	Bladder wall	Renal excretion	~1.5–2 h	ICRP 128
	Liver	GLUT transport	~1.5–2 h	ICRP 128
	Bone marrow	GLUT transport	~1.5–2 h	ICRP 128
F-18 NaF	Bone	Exchange into bone mineral	~2 h	ICRP 128
	Bladder wall	Renal excretion	~2 h	ICRP 128

3.3 References

Cherry, S. R., Sorenson, J. A., & Phelps, M. E. (2012). *Physics in nuclear medicine* (4th ed.). Elsevier.

Dash, A., Pillai, M. R. A., & Knapp, F. F. Jr. (2015). Radiopharmaceuticals for therapy: Current status and future prospects. *Quarterly Journal of Nuclear Medicine and Molecular Imaging*, 59(4), 297–309.

Garske, U., Sandström, M., Johansson, S., Granberg, D., Eriksson, B., Sundin, A., & Lundqvist, H. (2012). Lessons on flare, dose responses and advanced dosimetry in 200 patients treated with 177Lu-DOTATATE. *European Journal of Nuclear Medicine and Molecular Imaging*, 39(1), 99–109.

Hindorf, C., Glatting, G., Chiesa, C., Flux, G., Lassmann, M., & EANM Dosimetry Committee. (2021). EANM Dosimetry Committee guidance document: Dosimetry reporting for therapy with radiopharmaceuticals. *European Journal of Nuclear Medicine and Molecular Imaging*, 48(12), 4371–4385.

International Atomic Energy Agency. (2008). *Radiation protection in newer medical imaging techniques: PET/CT* (Safety Reports Series No. 58). IAEA.

International Commission on Radiological Protection. (2015). ICRP Publication 128: Radiation dose to patients from radiopharmaceuticals – A compendium of current information related to frequently used substances. *Annals of the ICRP*, 44(2S), 7–321.

Kao, Y. H., Steinberg, J. D., Tay, Y. S., Lim, G. K., Yan, S. W., Townsend, D. W., Takano, A., Luthra, S. K., Ng, D. C., & Khoo, J. B. (2013). Post-radioembolization yttrium-90 PET/CT - part 1: Diagnostic reporting. *EJNMMI Research*, 3(1), 56.

Klein Nulent, T. J. W., Valstar, M. H., de Keizer, B., Willems, S. M., Smit, L. A., Al-Mamgani, A., Smeele, L. E., & Vogel, W. V. (2019). Physiological distribution of PSMA-ligand uptake in the head and neck region. *Oral Diseases*, 25(6), 1541–1549.

Murthy, R., Nunez, R., Szklaruk, J., Erwin, W., Madoff, D. C., Gupta, S., Ahrar, K., Wallace, M. J., Cohen, A. M., Hicks, M. E., & Loyer, E. M. (2007). Yttrium-90 microsphere therapy for hepatic malignancy: Devices, indications, technical considerations, and potential complications. *RadioGraphics*, 27(6), 1541–1555.

Okamoto, S., Thieme, A., Allmann, J., D'Alessandria, C., Maurer, T., Retz, M., Tauber, R., Heck, M. M., Wester, H. J., & Eiber, M. (2017). Radiation dosimetry for 177Lu-PSMA I&T in metastatic castration-resistant prostate cancer: Evaluation of the impact of body mass index and body surface area. *Journal of Nuclear Medicine*, 58(1), 84–90.

Sandström, M., Garske, U., Granberg, D., Sundin, A., & Lundqvist, H. (2013). Individualized dosimetry of 177Lu-DOTATATE based on a single 7-day post-treatment SPECT/CT scan. *Medical Physics*, 40(11), 112504.

Sartor, O., de Bono, J., Chi, K. N., Fizazi, K., Herrmann, K., Rahbar, K., Tagawa, S. T., Nordquist, L. T., Vaishampayan, N., El-Haddad, G., Park, C. H., Beer, T. M., Armour, A., Pérez-Contreras, W. J., Desilva, M., Paik, P. K., Morris, M. J., & Krause, B. J. (2021). Lutetium-177–PSMA-617 for metastatic castration-resistant prostate cancer. *The New England Journal of Medicine*, 385(12), 1091–1103.

Strosberg, J., El-Haddad, G., Wolin, E., Hendifar, A., Yao, J., Chasen, B., Mittra, E., Kunz, P. L., Kulke, M. H., Jacene, H., Bushnell, D., O'Dorisio, T. M., Baum, R. P., Kulkarni, H. R., Caplin, M., Meyer, T., Hobday, T., Goldenberg, L., Houman, F., & NETTER-1 Trial Investigators. (2017). Phase 3 trial of 177Lu-Dotatate for midgut neuroendocrine tumors. *The New England Journal of Medicine*, 376(2), 125–135.

Valk, P. E., Bailey, D. L., Townsend, D. W., & Maisey, M. N. (2003). *Positron emission tomography: Basic science and clinical practice*. Springer.

Virgolini, I., Ambrosini, V., Bomanji, J. B., Baum, R. P., Fanti, S., Gabriel, M., Chiesa, C., Konijnenberg, M. W., Forrer, F., Papathanasiou, N. D., & others. (2010). Current knowledge on the use of 177Lu-DOTATATE and 177Lu-DOTATOC in neuroendocrine tumor therapy. *Journal of Nuclear Medicine*, 51(Suppl 2), 61S–66S.

Wadas, T. J., Pandya, D. N., & Zeglis, B. M. (2014). Targeting the PSMA receptor: Radioligands for imaging and therapy. *Current Topics in Medicinal Chemistry*, 13(23), 2759–2775.

Wieland, D. M., Brown, L. E., & Wu, J. L. (2005). Radiopharmaceutical chemistry. In R. E. Henkin, D. M. Boles, & G. L. Wagner (Eds.), *Nuclear medicine* (2nd ed., pp. 123–142). Mosby

.

CHAPTER 4

DOSIMETRIC METHODOLOGY

Nuclear medicine dosimetry provides a quantitative framework for estimating the absorbed dose delivered to tissues following the administration of radiopharmaceuticals. Accurate dosimetric assessment is essential for optimizing therapeutic efficacy while minimizing toxicity. Dosimetric formalism integrates physical, biological, and kinetic parameters, often employing standardized models such as MIRD schema or voxel-based approaches. Complementing this, imaging modalities such as planar scintigraphy, SPECT/CT, and PET/CT play a pivotal role in quantifying radionuclide biodistribution over time, forming the foundation for personalized, patient-specific dosimetric calculations.

4.1 Nuclear Medicine Dosimetric Formalism

Nuclear medicine dosimetric formalism defines the methods and mathematical models used to quantify absorbed radiation dose in organs and tissues during nuclear medicine procedures. It provides the foundation for precise therapy planning in radionuclide treatments and supports patient safety in diagnostic and therapeutic contexts.

Two main frameworks, MIRD and ICRP, are applied to calculate radiation doses from radionuclides within the body. Both estimates' ADs to specific organs but differ in objective, structure, and application. The primary distinctions between these two approaches appear in Table 4.1.

Table 4.1: Comparison of AD definition: MIRD vs ICRP in internal dosimetry.

Aspect	MIRD (Medical Internal Radiation Dose) Committee	ICRP (International Commission on Radiological Protection)
Origin & Purpose	• Developed by the Society of Nuclear Medicine and Molecular Imaging (SNMMI) MIRD Committee. • Personalized dosimetry in diagnostic and MRT.	• Established by the ICRP, a global authority on radiation protection. • Population based radiation protection and risk estimation.
Dosimetric Quantity	• AD (Gy), calculated using source-target organ models and S-values.	• AD (Gy), Equivalent dose (Sv), Effective dose (Sv).

Calculation Method	• Uses the MIRD schema: $D(T) = \sum \tilde{A}(S) \times S(T \leftarrow S)$ where i. $\tilde{A}(S)$: Cumulated activity in source organ. ii. $S(T \leftarrow S)$: Mean AD per unit cumulated activity from source to target organ.	• Uses dose coefficients derived from biokinetic and anatomical models, incorporating uncertainties and population variability. • Often presented as: $D = \tilde{A} \times DC.$ where i. DC: Dose coefficient (Sv Bq^{-1} or Gy Bq^{-1}), organ-specific.
Reference	• Example : MIRD Pamphlet No. 21.	• ICRP Publication 103.
Applications	• Diagnostic and therapeutic nuclear medicine planning and dosimetry.	• Radiation protection, regulatory limits, and health risk estimation.

4.1.1 Medical Internal Radiation Dose (MIRD)

This subchapter discusses the MIRD schema, a structured framework used to calculate internal radiation doses to organs or tissues following the administration of radiopharmaceuticals. It incorporates mathematical formulations and reference data that represent the physical, biological, and geometric characteristics of radionuclide distribution within the body. The approach enables consistent and precise dose estimation essential for evaluating therapeutic effectiveness, optimizing treatment planning, and maintaining safety in diagnostic and therapeutic nuclear medicine.

The MIRD schema consists of two principal components:

1) **S-values**: Define as the absorbed dose to a target region per unit time-integrated activity in a source region.

2) **Time-Integrated Activity (TIA, $\tilde{A}$)**: defines time-integrated activity as the total number of nuclear decays that occur in a source region over time.

Absorbed dose is obtained from the product of the time-integrated activity and the S-value:

$$D = \tilde{A} \times S \qquad \text{Equation 4-1}$$

Where the workflow involves deriving the $\tilde{A}$ from biokinetic models, evaluating the energy released per nuclear decay, and applying S-values to describe energy transfer from source regions to target tissues. as illustrated in Figure 4.1.

Hence, the MIRD formalism this with:

$$D(T) = \sum \tilde{A}(S) \times S(T \leftarrow S) \qquad \text{Equation 4-2}$$

Where D(T) is the AD to target organ, $\tilde{A}(S)$ is time-integrated activity in the source organ and S(T←S) the S-value, which gives the dose to target organ per unit cumulated activity in source organ.

Though AD does not account for biological impact (like radiation type), it is the foundational metric for internal dose assessments, regulatory compliance and personalized treatment planning in nuclear medicine.

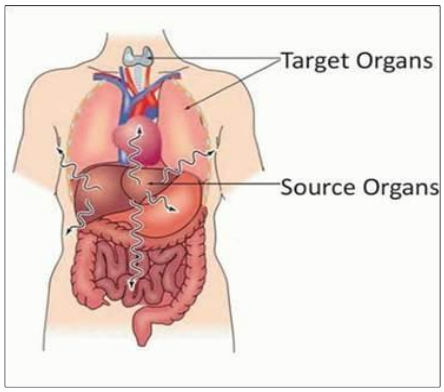

Figure 4.1: Source organ (S) and target organ (T).

This methodology combines biological data (such as organ uptake rates and clearance) with physical principles (including energy deposition from radiation) to provide a robust calculation of organ doses. Its application spans a variety of clinical and research contexts, from assessing radiation risks to optimizing personalized therapeutic regimens.

4.1.2 Organ Level Internal Dose Assessment (OLINDA)

OLINDA is a specialized software application designed for internal dosimetry calculations in nuclear medicine. It uses the well-established MIRD schema along with other advanced models to estimate radiation doses absorbed by specific organs and tissues. This software is widely employed in both clinical and research settings to evaluate the biodistribution of radiopharmaceuticals and their associated radiation exposure. Its primary goal is to facilitate accurate, efficient,

and standardized dose calculations, aiding in the planning and optimization of diagnostic imaging and MRT while ensuring patient safety.

OLINDA offers a comprehensive suite of features that make it a valuable tool for patient-specific dosimetry:

1) **Integration of Imaging Data**: The software allows users to input imaging data, such as SPECT or PET scans, to assess the spatial and temporal distribution of radiopharmaceuticals within the body. This enables the calculation of $\tilde{A}$, which is crucial for accurate dose estimation.

2) **Support for Radiopharmaceutical Characteristics**: OLINDA incorporates a database of commonly used radionuclides and radiopharmaceuticals, along with their decay properties, to streamline the dosimetry process. Users can also input custom radionuclide data for novel agents.

3) **Organ Specific and Whole-body Dose Calculations**: The software can compute radiation doses for individual organs as well as cumulative doses for the entire body, accounting for cross-organ dose contributions (source to target organ).

4) **Patient Specific Modeling**: By integrating patient specific data, such as organ masses and unique radiopharmaceutical kinetics, the tool allows for personalized dosimetry tailored to the individual's physiology and treatment protocol.

5) **User Friendly Interface and Reporting**: OLINDA provides an intuitive interface for entering data and generates detailed reports that summarize dose calculations, making it suitable for clinical documentation and regulatory compliance.

6) **Sphere Modeling**: A simplified dosimetric tool used to calculate the AD to small volumes of tissue (typically tumors or localized activity regions) by assuming the tissue is a uniform sphere of soft tissue containing a homogeneous distribution of radionuclide activity.

7) OLINDA received FDA clearance on June 15, 2004, making it the first internal dosimetry software available on the market.

4.1.3 Dosimetry Phantom Modelling

Dosimetry phantom modelling provides a structured approach for estimating radiation dose distribution within the human body by simulating anatomical and physiological characteristics. It enables standardized dose calculations that are

essential for validating computational methods and comparing different radionuclide therapies.

In computational phantoms, standard organ and body masses refer to predefined, reference values representing the average anatomical characteristics of a population subgroup (e.g., adult male, adult female, pediatric ages). These standard masses are essential for ensuring consistency, reproducibility, and comparability in internal dosimetry and radiation protection calculations. Both ICRP and MIRD have defined reference phantoms with standard masses for each organ and tissue.

The evolution of computational phantoms reflects advancements in imaging, computing power, and anatomical modelling, transitioning from simple representations to highly detailed and patient-specific models.

1) **Stylized (Mathematical) Phantoms**: First computational phantoms, the MIRD phantom, used simplified geometric shapes (e.g., ellipsoids, cylinders) to represent human anatomy. These models were easy to implement and computationally efficient but lacked anatomical realism.

2) **Voxel Based Phantoms**: With advancements in medical imaging technologies such as CT, voxel-based phantoms emerged. These models use three-dimensional (3D) arrays of cubic volume elements (voxels) derived from real human imaging data, significantly improving anatomical accuracy. Examples include the ICRP adult reference voxel phantoms, developed for both radiation protection and internal dosimetry applications **Hybrid Phantoms**: To increase anatomical flexibility while retaining realism, hybrid phantoms were developed using mathematical surfaces like non-uniform rational B-splines (NURBS) and polygon meshes. These allow for easy morphing to simulate various ages, body sizes, and organ motions.

4.1.4 Biokinetic Modelling

Biokinetic modeling is a technique used to simulate the biological behavior of radiopharmaceuticals within the human body. It helps predict the distribution, uptake, and elimination of these substances over time.

Several fitting techniques are used depending on the pharmacokinetic complexity of the radiopharmaceutical to accurately estimate the $\tilde{A}$. These include mono-exponential, bi-exponential, tri-exponential and trapezoidal integration.

While mono- and bi-exponential models are commonly used in clinical settings due to their simplicity and interpretability, trapezoidal integration with exponential tail offers flexibility when data is sparse. For complex or research-based

applications, tri-exponential is more suitable, although with higher data and computation requirements.

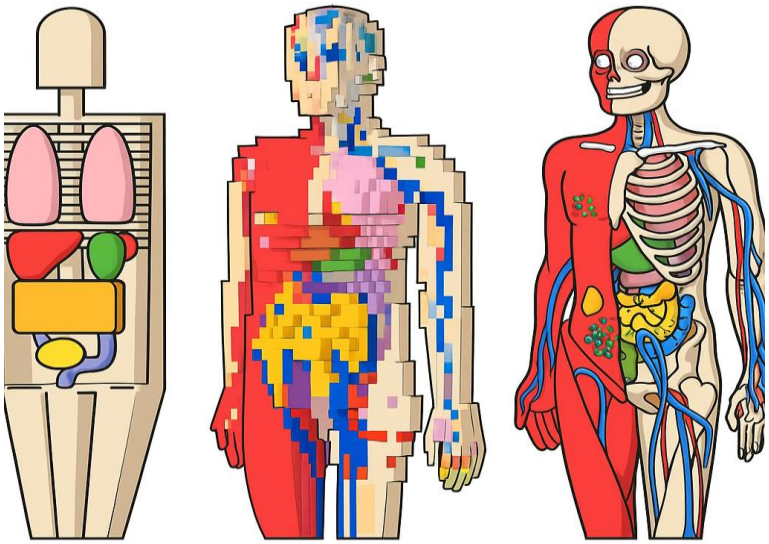

Figure 4.2 Graphical examples of a stylized, voxel, and hybrid adult male phantom.

Table 4.2: Time integration activity curve modeling methods.

Fitting Method	Description	Mathematical Model	Usage
Trapezoidal with exponential tail	• Non-parametric integration; fits exponential beyond last point	$\tilde{A}=\sum_{i=1}^{n-1}\frac{A(t_i)+A(t_{i+1})}{2}\times(t_{i+1}-t_i)+\int_{t_n}^{\infty}A(t)\,dt$	• Limited or noisy data, short imaging schedules
Mono-exponential	• Assumes single-phase clearance	$A(t) = A_1e^{-\lambda_1 t}$	• Suitable when tracer kinetics are dominated by one phase (e.g., simple renal clearance or rapid blood washout
Bi-exponential	• Models two clearance phases: fast and slow	$A(t) = A_1e^{-\lambda_1 t} + A_2e^{-\lambda_2 t}$	• Suitable for dual-phase behavior (e.g., rapid uptake followed by slow retention)
Tri-exponential	• Captures complex multi-phase kinetics	$A(t) = A_1e^{-\lambda_1 t} + A_2e^{-\lambda_2 t} + A_3e^{-\lambda_3 t}$	• Reserved for complex multi-compartment kinetics (e.g., bone marrow or tumor heterogeneity)

4.1.5 Model Evaluation Using Statistical Criteria

Selecting between mono-, bi-, or tri-exponential models requires objective statistical evaluation rather than visual judgment alone. Two widely applied metrics are the Akaike Information Criterion (AIC) and the adjusted coefficient of determination (adjusted R^2). These parameters provide complementary insights into the model's balance between goodness of fitness and complexity.

Table 4.3: Comparison of AIC and adjusted R^2 in model evaluation.

Aspect	AIC	Adjusted R^2
Purpose	• Quantifies the trade-off between model fit and complexity; penalizes additional parameters to prevent overfitting	• Measures how well the model explains variance in the data while adjusting for the number of fitted parameters
Formula	• $AIC = 2k - 2\ln(L)$ • Use the corrected form when data points remain limited: $AICc = AIC + (2k^2 + 2k) / (n - k - 1)$ where k = number of parameters L= maximum likelihood of the fitted model	• $R^2_{adj} = 1-(1-R^2)\frac{(n-1)}{(n-k-1)}$ where R^2_{adj}= coefficient of determination n= data points k= number of parameters
Scale and Direction	• Dimensionless; lower AIC indicates a better model	• Dimensionless; higher adjusted R^2 indicates a better model
Preferred Direction	• Choose model with lowest AIC	• Choose model with highest adjusted R^2
Best Practice	• Begin with mono-exponential; add components only if AIC decreases significantly and parameters remain physiologically meaningful	• Report adjusted R^2 along with AIC to confirm that complexity improves fit without inflating variance artificially

When applied to Time Activity Curve (TAC) fitting, both AIC and adjusted R^2 provide complementary information for selecting the most appropriate model.

In the Lu-177 TAC dataset, the mono-exponential model typically yields higher AIC values and lower adjusted R^2, indicating that it explains less of the data variance. Introducing a second exponential term often lowers the AIC significantly and increases the adjusted R^2, suggesting a better description of both uptake and clearance phases. However, adding a third component may only marginally improve adjusted R^2 while increasing model complexity, resulting in a smaller or even negative change in AIC.

Based on these criteria, the bi-exponential function is generally preferred when it offers a statistically justified improvement (Δ AIC > 10 and higher adjusted R^2) without introducing parameters lacking physiological meaning. This approach ensures model selection remains data-driven while maintaining biological plausibility.

4.2 Imaging Modalities for Dosimetric Methodology

Dosimetry in nuclear medicine has become increasingly critical as accurate measurement and assessment of radiation doses delivered to patients across various modalities. The goal is to quantify how much radioactivity localizes in organs or tumors over time to calculate the AD.

Several imaging modalities are employed for this purpose, each with distinct strengths. Key modalities include planar gamma camera imaging two-dimensional (2D) scintigraphy, SPECT/CT, and PET/CT.

4.2.1 Planar 2D scintigraphy

Planar scintigraphy represents the foundational imaging technique in nuclear medicine, utilizing gamma cameras to acquire 2D images of radiopharmaceutical distribution within the human body. This imaging modality, also known as planar gamma camera imaging, as shown in Figure 4.3, creates projection images based on the detection of gamma radiation emitted from administered radiopharmaceuticals.

The fundamental concept is based on the use of unsealed radionuclide sources in radiopharmaceutical form, where the ionizing radiation emitted during decay can be quantitatively detected, measured, and imaged in vivo using gamma camera systems. Planar scintigraphy offers functional assessment of organ systems by depicting the biodistribution and kinetic behavior of targeted radiopharmaceuticals. However, because of its higher level of uncertainty and limited spatial information, it has largely been replaced by SPECT imaging, which provides improved quantification and 3D localization.

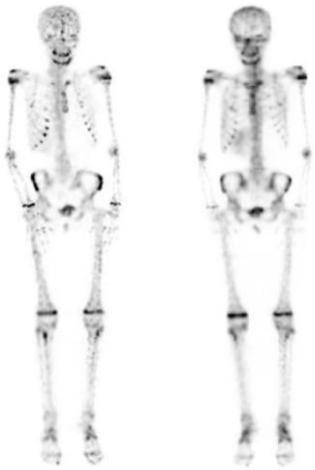

Figure 4.3: Whole body bone planar scintigraphy using radiopharmaceuticals Tc-99m MDP.

4.2.2 SPECT/CT Imaging Dosimetry

SPECT/CT has revolutionized nuclear medicine dosimetry by providing integrated functional and anatomical imaging capabilities. The methodology for SPECT/CT dosimetry involves highly patient-specific tumor dosimetry utilizing 3D ordered-subset expectation-maximization (OSEM) reconstruction and CT-defined tumor outlines at each time point.

The quantification process for SPECT/CT dosimetry includes several critical steps as Table 4.4.

Table 4.4: Summarizing the quantification process for SPECT/CT dosimetry.

Step	Description
1. Activity Measurement	Radiopharmaceutical activity is measured with a dose calibrator to provide accurate dosimetry input, with routine checks against sources traceable to a primary standard to maintain measurement validity
2. Image Acquisition	Patient data are acquired using standardized SPECT CT protocols with fixed time points and reconstruction parameters, with partial volume correction factors determined and applied, particularly for small lesions
3. Image Correction & Registration	Apply attenuation, scatter, and resolution recovery corrections and align images across time points
4. Image Segmentation	Segment ROIs or VOIs from reconstructed and corrected images
5. Time-Activity Curve Generation	Extract activity values over time to generate TACs
6. AD Calculation	Integrate TACs and apply dosimetric models such as MIRD or voxel-based methods to calculate ADs

Each step in this chain propagates dosimetry inaccuracy and precision, making accurate activity quantification essential for reliable dose calculations as shown in Figure 4.4.

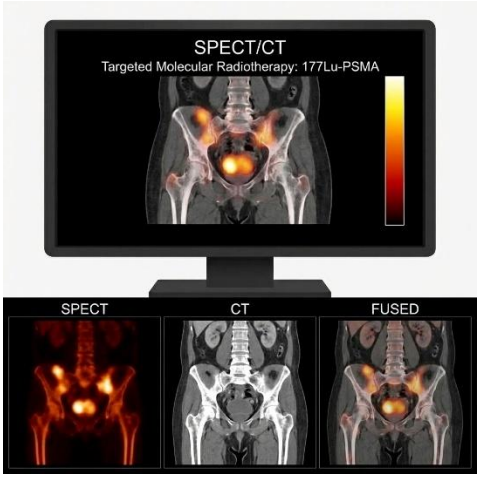

Figure 4.4: SPECT/CT imaging for targeted molecular radiotherapy in metastatic castration-resistant prostate cancer. (Image generated using artificial intelligence).

The AD depends on patient-specific biokinetics, tumor volume, radionuclide such as Lu-177 and I-131, and imaging time points. A complete dosimetry report includes time-activity plots, integration methods, software used, and S-values or MC input. Based on the MIRD Pamphlet No. 21, A generalized schema for radiopharmaceutical dosimetry for standardization of nomenclature as shown in Table 4.5.

Table 4.5: A cumulated activity and AD calculation in SPECT/CT modalities.

Region/Organ	$\tilde{A}$ (MBq h^{-1})	AD (Gy)
Liver Tumor	180	12.5
Kidney (left)	95	4.2
Bone Marrow	65	1.8

4.2.3 PET/CT Dosimetry Methodology

PET/CT dosimetry requires patient specific approaches to characterize radiation exposure accurately. The methodology involves calculating both PET and CT organ doses using patient-specific data, with PET dose calculated by modifying standard reference phantoms with patient-specific organ mass, and CT dose calculated using patient-specific data in specialized software systems.

Studies have demonstrated that mean patient-specific effective doses from F-18 FDG PET/CT procedures can range from approximately 9.0 ± 1.6 mSv for the PET component, with total effective doses varying significantly based on CT technique employed. For diagnostic quality CT protocols, total effective doses

can reach 24.4 ± 4.3 mSv, while standard registration CT protocols typically result in lower total doses of 14 ± 1.3 mSv and and low-dose CT for attenuation correction purposes even can lead to doses of 1 mSv and below.

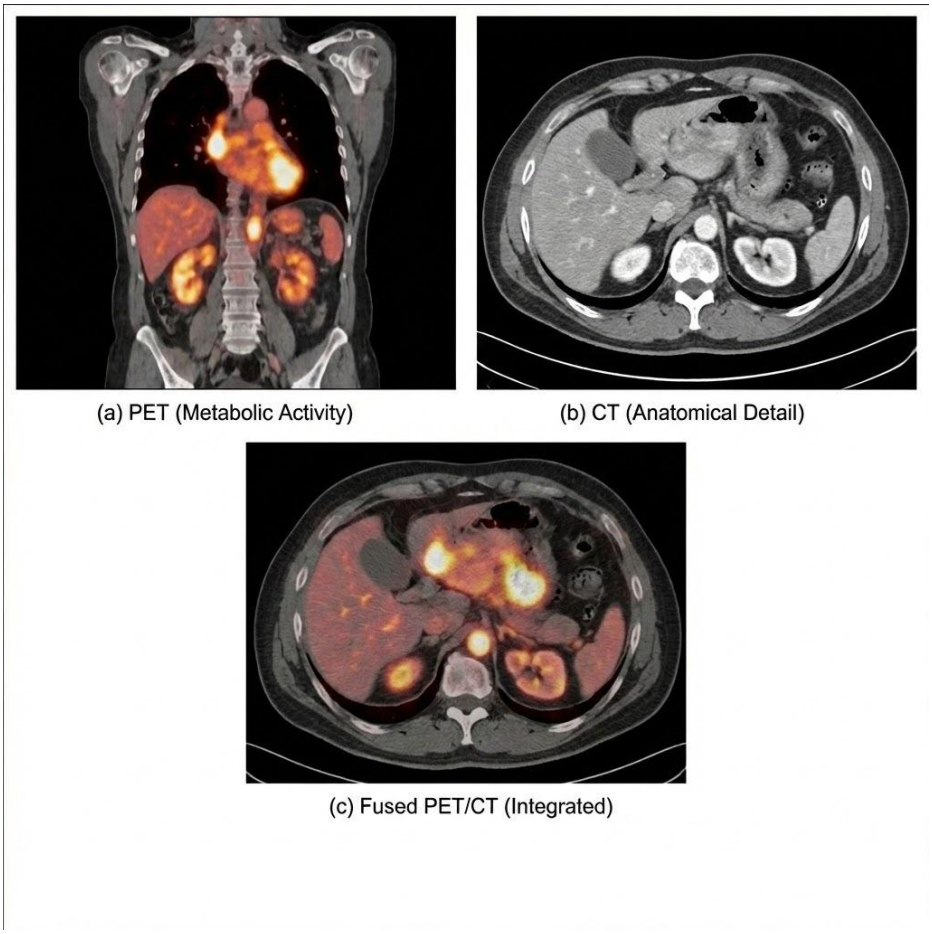

Figure 4.5: Example of multimodal imaging combining PET, CT, and fused PET/CT images. The PET image (a) shows metabolic activity based on radiotracer uptake, the CT image (b) provides anatomical detail, and the fused PET/CT image (c) integrates both datasets, allowing precise localization of functional abnormalities within anatomical structures. (Image generated using artificial intelligence).

Among these imaging dosimetric modalities as shown in Figure 4.4, SPECT/CT is highlighted for its ability to provide 3D activity distributions with anatomical context, which is crucial for patient-specific dosimetric calculations. The general dosimetric methodology (e.g. MIRD formalism) relies on imaging to estimate the time-integrated activity in source regions, linking the radiopharmaceutical's uptake kinetics to AD.

The following sections summarize each imaging approach and how SPECT/CT integrates into dosimetric workflows according to current standards with emphasis on IAEA guidance.

Table 4.6 shows comparison table highlighting the three primary imaging modalities used in internal dosimetry planar scintigraphy, SPECT/CT, and PET/CT featuring example images, concise descriptions, and their key diagnostic characteristics.

Table 4.6: Comparison the three main imaging modalities used in internal dosimetry.

Imaging Modality	Description	Key Features
Planar Scintigraphy (2D Gamma Camera Imaging)	• A 2D projection image using a gamma camera to detect the distribution of radiotracers	• Overlapping tissues • Quick whole-body imaging • Low resolution
SPECT/CT	• Provides 3D functional imaging with anatomical co-registration from CT	• Quantitative 3D • Attenuation correction via CT • Organ level segmentation • Widely used in MRT dosimetry
PET/CT	• Combines PET tracer uptake mapping with CT anatomy for high-precision imaging	• High resolution (~4 mm) • Superior quantification • Ideal for theranostic • Limited by tracer availability

4.3 Non-imaging modalities for dosimetric methodology

Non-imaging dosimetric approaches for radiopharmaceutical therapy are defined by the direct longitudinal measurement of activity in the blood and the whole body, rather than relying on scintigraphy imaging. This process typically commences with the administration of a tracer activity intended specifically for dosimetric evaluation. Following administration, serial blood samples are collected and whole-body radioactivity is monitored at predefined intervals over several days using external counting equipment, such as a calibrated detector in a fixed geometry as depicted in .

As illustrated in , clinical quantification for internal dosimetry relies on two fundamental non-imaging instruments: the dose calibrator and the well counter. While imaging modalities (such as SPECT or PET) delineate spatial distribution, these instruments are indispensable for the absolute measurement of activity and the verification of patient-specific doses.

The dose calibrator is primarily used to quantify radiopharmaceutical activity prior to patient administration, providing accurate input for systemic biokinetic modelling.

In contrast, the well counter is employed for high-sensitivity measurement of biological samples, such as blood or urine, following injection to determine time-dependent activity fractions

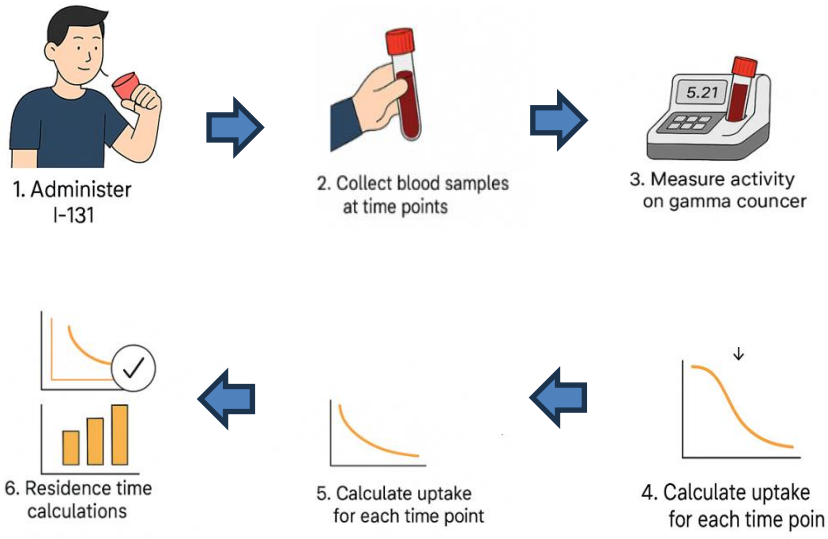

Figure 4.6: Workflow for determining blood $\tilde{A}$ following I-131 administration, including sample collection, gamma counting, uptake calculation, and integration of activity–time data for dosimetric analysis.

The reliability, traceability, and precision of these devices form the analytical foundation for accurate AD calculations.

Non-Imaging Modalities	Primary Use	Output Unit	Example sample measurements	Advantages	Disadvantages
Dose Calibrator 	Measurements of high radioactivity	Bq/Ci	MRT radioactivity dose	Accurate radioactivity quantification	Limited sensitivity for very low activity samples

Well Counter/Thyroid Uptake	Measurements of low radioactivity	Bq/cps	Blood, Urine, I-131 thyroid uptake	High sensitivity for low radioactivity	Not suitable for high activity measurements

Figure 4.7: Two fundamental instruments used for non-imaging modalities.

4.4 References

Al-Okshi, A., Lindh, C., Salé, H., Gunnarsson, M., & Rohlin, M. (2015). Effective dose of cone beam CT (CBCT) of the facial skeleton: A systematic review. *The British Journal of Radiology, 88*(1045), 20140658.

Bolch, W. E., Lee, C., Wayson, M., et al. (2010). Hybrid computational phantoms for medical dose reconstruction. *Radiation and Environmental Biophysics, 49*, 155–168.

Coleman, D., Griffin, K. T., & Dewji, S. A. (2023). Stylized versus voxel phantoms: Quantification of internal organ chord length distances. *Physics in Medicine & Biology, 68*(5), 055020.

Cristy, M., & Eckerman, K. F. (1987). *Specific absorbed fractions of energy at various ages from internal photon sources. I. Methods* (ORNL/TM-8381/V1). Oak Ridge National Laboratory.

Dewaraja, Y. K., Wilderman, S. J., Koral, K. F., Kaminski, M. S., & Avram, A. M. (2009). Use of integrated SPECT/CT imaging for tumor dosimetry in I-131 radioimmunotherapy: A pilot patient study. *Cancer Biotherapy & Radiopharmaceuticals, 24*(4), 417–426.

Garske-Román, U., Sandström, M., Fröss-Baron, K., et al. (2018). Individualized dosimetry of kidney and bone marrow in patients undergoing 177Lu-DOTA-octreotate treatment. *European Journal of Nuclear Medicine and Molecular Imaging, 45*(13), 2123–2135.

Hindorf, C., Glatting, G., Chiesa, C., et al. (2021). EANM Dosimetry Committee guidelines for dosimetry reporting in therapy using radiopharmaceuticals. *European Journal of Nuclear Medicine and Molecular Imaging, 48*(12), 4371–4385.

Hofman, M. S., Violet, J., Hicks, R. J., et al. (2018). [177Lu]-PSMA-617 radionuclide treatment in patients with metastatic castration-resistant prostate cancer (LuPSMA trial): A single-centre, single-arm, phase 2 study. *The Lancet Oncology, 19*(6), 825–833.

International Commission on Radiological Protection (ICRP). (2009). *Adult reference computational phantoms* (ICRP Publication 110). *Annals of the ICRP, 39*(2).

Lee, C., Lodwick, D., Hurtado, J., Pafundi, D., Lee, C., & Bolch, W. E. (2019). The UF/NCI family of hybrid computational phantoms representing the current US population of male and female children, adolescents, and adults. *Physics in Medicine & Biology, 64*(1), 015010.

Martin, C. J. (2011). Personal dosimetry for interventional operators: When and how should monitoring be done? *The British Journal of Radiology, 84*(1003), 639–648.

Meghzifene, A., Dance, D. R., McLean, D., & Kramer, H.-M. (2010). Dosimetry in diagnostic radiology. *European Journal of Radiology, 76*(1), 11–14.

Ramonaheng, K., Qebetu, M., Ndlovu, H., Swanepoel, C., Smith, L., Mdanda, S., Mdlophane, A., & Sathekge, M. (2024). Activity quantification and dosimetry in radiopharmaceutical therapy with reference to 177Lu. *Frontiers in Nuclear Medicine, 4*, 1355912.

Segars, W. P., Sturgeon, G., Mendonca, S., Grimes, J., & Tsui, B. M. W. (2010). 4D XCAT phantom for multimodality imaging research. *Medical Physics, 37*(9), 4902–4915.

Sisson, J. C., Avram, A. M., & Thrall, J. H. (2003). Dose response and dosimetry in the treatment of thyroid cancer. *Seminars in Nuclear Medicine, 33*(1), 30–38.

Stabin, M. G., & Siegel, J. A. (2003). Physical models and dose factors for use in internal dose assessment. *Health Physics, 85*(3), 294–310.

Stabin, M. G., Sparks, R. B., & Crowe, E. (2005). OLINDA/EXM: The second-generation personal computer software for internal dose assessment in nuclear medicine. *Journal of Nuclear Medicine, 46*(6), 1023–1027.

Strigari, L., Sciuto, R., Rea, S., et al. (2014). Radiobiological optimization of radioembolization with 90Y-microspheres: A review. *European Journal of Nuclear Medicine and Molecular Imaging, 41*(3), 449–465.

Vano, E., Frija, G., Loose, R., Paulo, G., Efstathopoulos, E., Granata, C., & Andersson, J. (2021). Dosimetric quantities and effective dose in medical imaging: A summary for medical doctors. *Insights into Imaging, 12*(1), 99.

CHAPTER 5

RADIONUCLIDE DIAGNOSTIC AND THERAPY DOSIMETRY

Dosimetry forms the quantitative foundation of nuclear medicine, linking administered activity to the resulting absorbed radiation dose within biological tissues. This chapter examines the methods, principles, and applications of dosimetry in both diagnostic and therapeutic nuclear medicine. It focuses on the characterization of radionuclide behavior in vivo, the use of time and activity data to estimate organ and lesion doses, and the application of standardized models for internal dose assessment.

5.1 Diagnostic Dosimetry

Diagnostic dosimetry in nuclear medicine is important for estimating how much radiation a patient measurement is needed to keep patients safe, especially children and pregnant women. Even though the doses are low, accurate dose assessment must follow the ALARA principle by adjusting the amount of radioactivity used to get clear images with the least radiation. Additionally, dosimetry plays a key role in dose optimization - balancing image quality and diagnostic value while minimizing unnecessary radiation.

In Good Practice such Quality Management Audits in Nuclear Medicine (QUANUM) ,diagnostic dosimetry is required for each diagnostic procedure and protocol to ensure accurate dose assessment, optimize patient safety, and support quality assurance in nuclear medicine practices.

It is also needed when developing new radiopharmaceuticals, as health authorities like the US Food and Drug Administration (FDA) and European Medicines Agency (EMA) require dose information for approval. Dosimetry helps compare different imaging methods and supports personalized care by allowing dose changes for sensitive patients or those who need many scans. Overall, it ensures nuclear imaging is safe and effective.

Diagnostic dosimetry in nuclear medicine estimates how much radiation a patient's organs receive after a radiopharmaceutical is given. By using dose coefficients from ICRP Publication 128, the AD to each organ can be calculated by multiplying the administered activity with the corresponding dose coefficient for the organ as shown in Equation 5-1.

This provides the estimated radiation dose to that organ, aiding in the evaluation of patient exposure and the optimization of diagnostic protocols.

$$AD\ (mGy) = A_o\ (MBq) \times Dose\ Coefficient\ (mGy\ MBq^{-1}) \qquad \text{Equation 5-1}$$

ICRP Publication 128, "Radiation Dose to Patients from Radiopharmaceuticals" provides a clear and structured summary for each radiopharmaceutical. It includes a description of how the substance behaves in the body, how it moves through organs over time, and the radiation it delivers. These key points are shown in Figure 5.1 to help explain the overall dosimetry process.

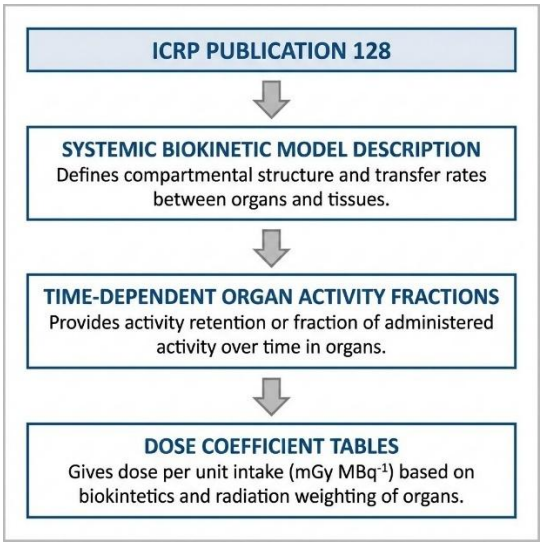

Figure 5.1: Framework of ICRP Publication 128 for internal dosimetry, illustrating the sequential process from systemic biokinetic modeling to time-dependent organ activity estimation and derivation of dose coefficients per unit intake. This three-step approach links biological kinetics with standardized organ specific coefficients for diagnostic internal dosimetry.

In addition, the biokinetic data can be explained in several key parameters to show how radiopharmaceuticals behave inside the body. The source organ (S) refers to the tissue where the radionuclide resides and emits radiation. The fractional distribution (F_s) denotes the proportion of the administered activity that localizes in that organ. Biological half-times (T) describe how quickly the radionuclide is cleared from the organ through biological processes. In cases where clearance involves multiple pathways, component fractions (α) represent the relative contribution of each pathway. Finally, the $\widetilde{A}_s$ in the source organ, reflecting the total amount of radionuclide emissions over time and serving as a key input for AD calculations.

Below are some examples for diagnostic dosimetry.

a. Fluorine 18 fluoro-2-deoxy-D-glucose (F-18 FDG).

   To assess the AD from F-18 FDG, metabolic activity, such as the brain, heart, and cancer cells, use biokinetic models to track how the tracer is distributed, retained, and cleared as presented in Table 5.1.

Table 5.1: Biokinetic data for F-18 FDG (adapted from ICRP 128).

Organ (S)	Fs	T(h)	α	$\tilde{A}$ (h)
Brain	0.08	∞	1.000	0.210
Heart Wall	0.04	∞	1.000	0.110
Lungs	0.03	∞	1.000	0.079
Liver	0.05	∞	1.000	0.130
Other Organ and tissues	0.80	0.2 1.5 ∞	0.075 0.225 0.700	1.700
Urinary Bladder contents	0.24			
Adult, 15 Years, 10 Years				0.26
5 Years				0.23
1 years				0.16

These biokinetic models generate standard $\tilde{A}$, showing how the amount of radioactivity in each organ changes over time. By integrating these curves, these models generate standard $\tilde{A}$ for each organ. These times are then used with dose coefficients (based on physical decay and organ geometry) to calculate the AD in mGy or the effective dose in mSv in Table 5.2 , which reflects overall risk.

Table 5.2: Dose coefficients for F-18 FDG (adapted from ICRP 128).

	AD per unit Activity administered (mGy MBq^{-1})				
Organ	Adult	15 Years	10 Years	5 Years	1 Years
Adrenals	1.20E-02	1.60E-02	2.40E-02	3.90E-02	7.10E-02
Bone surfaces	1.10E-02	1.40E-02	2.20E-02	3.40E-02	6.40E-02
Brain	3.80E-02	3.90E-02	4.10E-02	4.60E-02	6.30E-02
Breast	8.80E-03	1.10E-02	1.8E -02	2.90E-02	5.60E-02
Gallbladder Wall	1.30E-02	1.60E-02	2.4E -02	3.70E-02	7.00E-02
Heart Wall	6.70E-02	8.70E-02	1.30E-01	2.10E-01	3.80E-01
Kidneys	1.70E-02	2.10E-02	2.90E-02	4.50E-02	7.80E-02
Liver	2.10E-02	2.80E-02	4.2E -02	6.30E-02	1.20E-01
Lungs	2.00E-02	2.90E-02	4.1E -02	6.20E-02	1.20E-01
Muscles	1.00E-02	1.30E-02	2.00E-02	3.30E-02	6.20E-02
Oesophagus	1.20E-02	1.5E--02	2.20E-02	3.50E-02	6.60E-02
Ovaries	1.40E-02	1.8E -02	2.70E-02	4.3E -02	7.60E-02
Pancreas	1.3E -02	1.60E-02	2.60E-02	4.00E-02	7.60E-02

Red Marrow	1.10E-02	1.40E-02	2.10E-02	3.20E-02	5.90E-02
Skin	7.80E-03	9.60E-03	1.5E -02	2.60E-02	5.00E-02
Spleen	1.10E-02	1.40E-02	2.10E-02	3.50E-02	6.60E+00
Thyroid	1.00E-02	1.30E-02	2. 16-02	3.40E-02	6.50E-02
Uterus	1.80E-02	2.2 E- 02	3.6E -02	5.40E-02	9.0E- 02
Remaining Organs	1.2E- 02	1.5 E-02	2.40E-01	3.80E-02	6.40E-02
Effective Dose (mSv MBq^{-1})	1.90E-02	2.40E-02	3.70E-02	5.60E-02	9.50E-02

Estimate AD of kidneys organ for F-18 FDG for 14 years old patient if the administered activity is 156 MBq?

Based on

$$AD\ (mGy) = Ao\ (MBq) \times \text{Dose Coefficient}\ (mGy\ MBq\text{-}1) \qquad \text{Equation 5-1}$$

the AD to the kidneys is determined by multiplying the administered activity by the dose coefficient for F-18 FDG in the kidneys

$AD\ (mGy) = 156\ MBq \times 7.80 \times 10^{-2}\ mGy\ MBq^{-1}$

The AD of kidneys organ for 14 years old male patient is 12.17 mGy

b. Technetium –99m -labeled phosphates and phosphonates

Tc-99m bone scans utilize phosphate and phosphonate-based radiopharmaceuticals—such as methylene diphosphonate (MDP) and hydroxy methylene diphosphonate (HDP) which have a high affinity for bone tissue and are widely used in nuclear medicine for skeletal imaging. After intravenous injection, around 50% of the tracer localizes in the bone within 15 minutes, with retention characterized by two biological half-times: 2 hours (30%) and 3 days (70%), while a small portion (~2%) is taken up by the kidneys and excreted renally. These agents accumulate in areas of increased osteoblastic activity and bone remodeling, making Tc-99m bone scans particularly valuable in oncology for detecting bone metastases from cancers such as prostate, breast, and lung. Metastatic lesions often present as areas of abnormal tracer uptake (hot spots), allowing early detection before structural changes occur as shown in Table 5.3.

Table 5.3: Biokinetic data for Tc-99m-labelled phosphates and phosphonates (adapted from ICRP Publication 53).

Organ (S)	Fs	T(h)	α	$\tilde{A}$ (h)
Normal Uptake and Excretion				
Total Body (Exc Urinary Bladder content)	1.0	0.5	0.3	4.1
		2.0	0.3	
		72	0.4	
Bone	0.5	0.25	-1.0	3.0
		2.0	0.3	
		72	0.7	
Kidneys	0.02	0.5	0.3	0.13
		2.0	0.3	
		72	0.4	
Urinary Bladder	1.0			
Adult, 15 Years, 10 Years				1.2
5 Years				0.97
1 Year				0.63
High bone uptake and/or severely impaired kidneys function				
Total Body	1.0	∞	1.0	8.7
Bone	0.7	0.25	-1.0	5.8
		∞	1.0	

Biokinetic data for Tc-99m-labelled phosphates and phosphonates provide the basis for calculating radiation dose coefficients, enabling the estimation of organ-specific and effective doses in nuclear medicine procedures as shown in Table 5.4.

Table 5.4: Dose coefficients for Tc-99m-labelled phosphates and phosphonates under normal uptake and excretion conditions (adapted from ICRP Publication 53).

Organ	AD per unit Activity administered (mGy MBq^{-1})				
	Adult	15 Years	10 Years	5 Years	1 Years
Normal Uptake and Excretion					
Adrenals	2.10E-03	2.60E-03	3.80E-03	5.80E-03	1.10E-02
Bone surfaces	3.40E-02	1.50E-02	2.30E-02	3.80E-02	8.20E-02
Brain	1.70E-03	2.00E-03	2.80E-03	4.20E-03	5.90E-03
Breast	6.90E-04	8.60E-04	1.30E-03	2.10E-03	4.00E-03
Gallbladder Wall	1.40E-03	1.80E-03	3.30E-03	4.30E-03	6.50E-03
Heart Wall	1.20E-03	1.50E-03	2.20E-03	3.30E-03	5.90E-03
Kidneys	7.20E-03	8.70E-03	1.20E-02	1.80E-02	3.10E-02

Liver	1.20E-03	1.6E—03	2.40E-03	3.60E-03	6.40E-03
Lungs	1.20E-03	1.60E-03	2.30E-03	3.50E-03	6.70E-03
Muscles	1.80E-03	2.20E-03	3.30E-03	4.70E-03	7.70E-03
Oesophagus	1.00E-03	1.30E-03	1.90E-03	2.90E-03	5.10E-03
Ovaries	3.60E-03	4.50E-03	6.50E-03	8.60E-03	1.20E-02
Pancreas	1.60E-03	2.00E-03	3.00E-03	4.50E-03	7.90E-03
Red Marrow	5.90E-03	5.40E-03	8.80E-03	1.70E-02	3.60E-02
Skin	9.90E-04	1.30E-03	1.90E-03	3.00E-03	5.30E-03
Spleen	4.70E-02	5.90E-02	8.70E-02	1.10E-01	1.30E+00
Thyroid	1.30E-03	1.50E-03	2.20E-03	3.40E-03	5.40E-03
Uterus	6.20E-03	7.50E-03	1.10E-02	1.40E-02	1.80E-02
Remaining Organs	1.90E-03	2.30E-03	3.40E-03	5.00E-03	7.70E-03
Effective Dose ($mSv\ MBq^{-1}$)	4.9E03	5.7E03	8.6E03	1.2E02	1.8E02

Table 5.5: Radiation dose coefficients for Tc-99m-labelled phosphates and phosphonates under conditions of high bone uptake and/or severely impaired kidney function (adapted from ICRP Publication 53).

Organ	AD per unit Activity administered ($mGy\ MBq^{-1}$)				
	Adult	15 Years	10 Years	5 Years	1 Years
High bone uptake and/or severely impaired kidneys function					
Adrenals	4.00E-03	5.00E-03	7.20E-03	1.10E-02	2.10E-02
Bone surfaces	6.50E-02	3.00E-02	4.50E-02	7.40E-02	1.60E-01
Brain	3.70E-03	4.50E-03	6.30E-03	9.60E-03	1.40E-02
Breast	1.70E-03	2.10E-03	3.20E-03	5.00E-03	9.60E-03
Gallbladder Wall	2.80E-03	3.60E-03	5.90E-03	8.5E -03	1.30E-02
Heart Wall	2.90E-03	3.60E-03	5.20E-03	7.70E-03	1.40E-02
Kidneys	2.90E-03	3.70E-03	5.60E-03	8.70E-03	1.60E-02
Liver	2.60E-03	3.30E-03	4.90E-03	7.40E-03	1.40E-02
Lungs	2.9E -03	3.70E-03	5.40E-03	8.10E-03	1.50E-02
Muscles	2.90E-03	3.60E-03	5.30E-03	8.00E-03	1.50E-02
Oesophagus	2.50E-03	3.10E-03	4.50E-03	7.00E-03	1.20E-02
Ovaries	3.20E-03	4.10E-03	5.80E-03	8.80E-03	1.60E-02
Pancreas	3.20E-03	4.00E-03	5.80E-03	8.80E-03	1.60E-02
Red Marrow	1.10E-02	1.00E-02	1.70E-02	3.20E-02	7.10E-02
Skin	1.90E-03	2.40E-03	3.70E-03	6.00E-03	1.10E-02
Spleen	2.60E-03	3.50E-03	5.40E-03	7.30E-03	1.50E-02
Thyroid	3.10E-03	3.70E-03	5.30E-03	8.20E-03	1.40E-02
Uterus	2.90E-03	3.70E-03	5.30E-03	8.10E-03	1.50E-02
Remaining Organs	3.00E-03	3.70E-03	5.50E-03	8.60E-03	1.50E-02
Effective Dose ($mSv\ MBq^{-1}$)	4.3E-03	4.5E-03	6.8E-03	1.1E-02	2.2E-02

For example, to estimate the AD to the thyroid for a 30-year-old male following the administration of 740 MBq of Tc-99m MDP.

$AD\ (mGy) = A_o\ (MBq) \times \text{Thyroid dose coefficient}\ (mGy\ MBq^{-1})$
$AD = 740 \times 3.10 \times 10^{-3} = 2.29\ mGy.$

The estimated AD to the thyroid for a 30-year-old male patient receiving 740 MBq of Tc-99m MDP is 2.29 mGy.

5.2 Therapy Dosimetry

Therapy dosimetry in nuclear medicine refers specifically to the measurement and calculation of the absorbed radiation dose delivered to organs and tumors during MRT. Unlike external beam therapy, nuclear medicine therapy involves systemic or localized administration of radiopharmaceuticals that target specific tissues (usually tumors), making dosimetry more complex but critical for personalized MRT. Therapy dosimetry assessment is crucial for maximizing the radiation dose absorbed by the tumor to enhance treatment effectiveness, while simultaneously minimizing the dose to normal organs to reduce the risk of toxicity. Each serves a distinct purpose in treatment planning and evaluation.

5.2.1 Organ Dosimetry

Organ based dosimetry models such as the MIRD schema offer a standardized approach for estimating ADs to target organs by considering the activity within source organs. These models utilize simplified anatomical assumptions and pre-calculated S-values to determine dose distribution. The relationship is discussed as in chapter 2.

Accurate identification of source and target organs is critical, as the biodistribution of radiopharmaceuticals affects both radiation delivery and dose estimation. This process typically involves anatomical imaging to localize uptake regions within the body.

Organ mass correction adjusts standard S-values or AD calculations based on actual organ volumes derived from patient imaging. This ensures personalized dosimetry that reflects anatomical variability among patients.

$$S_{corrected} = S_{reference} \times \frac{m_{reference}}{m_{patients}} \qquad \text{Equation 5-2}$$

Whole-body and planar imaging are commonly used to estimate the $\tilde{A}$ of radionuclides in organs by tracking the activity distribution over time. $\tilde{A}$ are

derived to calculate the total number of disintegrations, a key parameter for dosimetry.

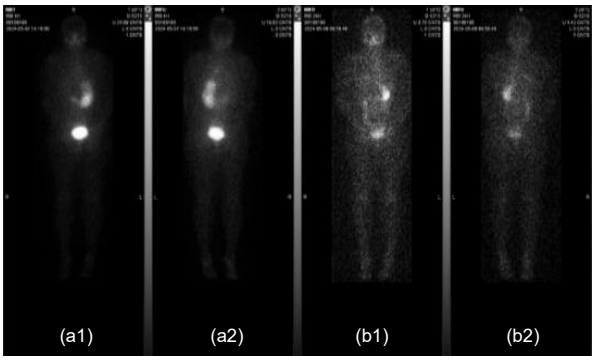

Figure 5.2: Conjugate views were obtained with scans acquired approximately 4 hours post-intravenous injection of 2 MBq of I-131, capturing the anterior view (a1) and posterior view (a2). Additional scans were taken 24 hours later, capturing the anterior view (b1) and posterior view (b2).

The low spatial resolution of planar imaging leads organ-based dosimetry to assume a uniform distribution of activity within organs. However, this overlooks intra-organ heterogeneity and individual functional differences, potentially causing errors in dose estimation.

5.2.2 Tumor Dosimetry

Tumor dosimetry begins with accurate delineation of volumes of interest (VOIs) using anatomical (CT) or functional imaging modalities such as SPECT and PET. VOI definition directly influences the precision of activity quantification and AD estimation.

Quantifying activity within a tumor involves image calibration and segmentation to obtain activity concentrations over time. These data points are used to generate $\tilde{A}$ that allow integration of activity and calculation of cumulated activity.

$$\text{Tumor activity (kBq mL}^{-1}) = \frac{\text{Tumor (cps)}}{\text{Sensitivity (cps kBq}^{-1} \times \text{mL)}} \qquad \text{Equation 5-3}$$

Voxel-based dosimetry calculates AD on a 3D voxel-by-voxel basis, providing detailed spatial dose distributions within the tumor. This approach is more sensitive to heterogeneous uptake patterns and improves dose accuracy compared to organ-based dosimetry methods.

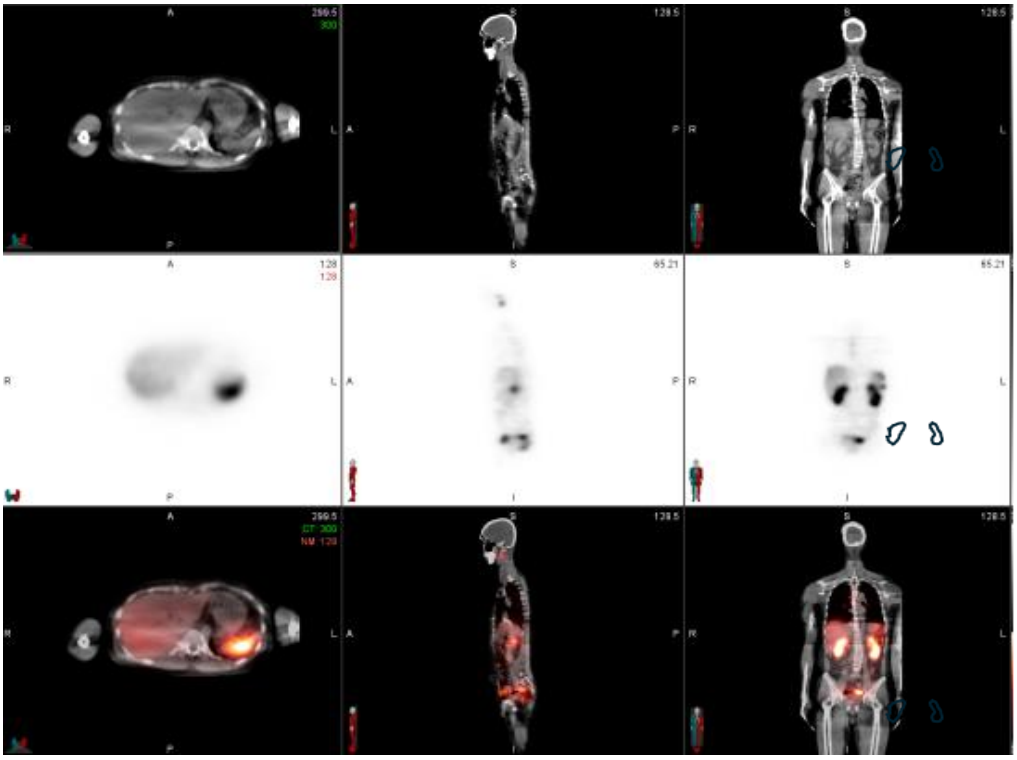

Figure 5.3: SPECT/CT imaging of a patient post MRT showing axial, sagittal, and coronal views.

Biological effective dose (BED) accounts for the radiobiological effects of dose rate and repair kinetics, offering a more clinically relevant parameter than AD alone. Tumor control probability (TCP) models predict the likelihood of tumor control based on the delivered BED, supporting treatment optimization

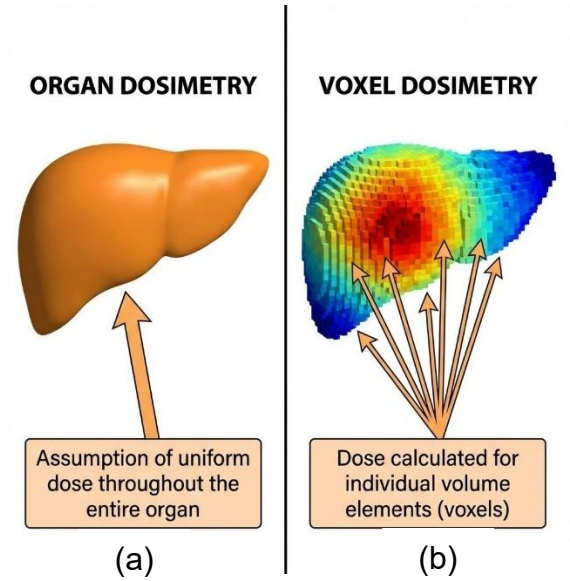

Figure 5.4: (a) Organ dosimetry (average AD across the organ). (b) Voxel dosimetry (sum of voxels across the organ for AD).

.

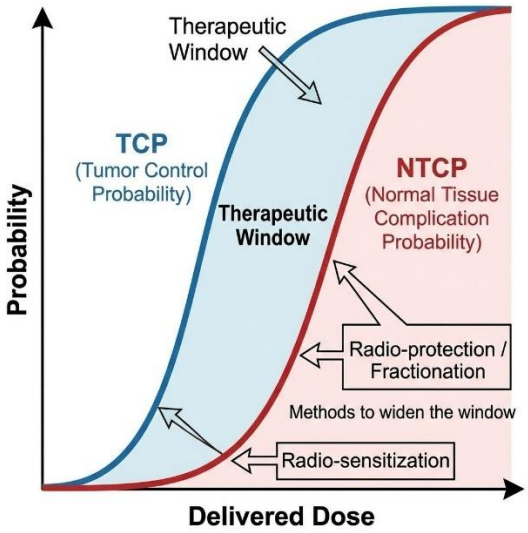

Figure 5.5: Illustration of the therapeutic window. For an identical delivery dose, the curves show the difference between TCP and NTCP.

5.2.3 Partial Volume Effect (PVE) and Correction (PVC)

The accurate assessment of dose to small, heterogeneous target volumes is frequently complicated by the Partial Volume Effect (PVE). Understanding this effect and applying appropriate Partial Volume Correction (PVC) is critical for achieving the intended clinical outcome, particularly in high-precision treatments like Stereotactic Body Radiation Therapy (SBRT).

a) Understanding the Partial Volume Effect (PVE)

The partial volume effect (PVE) represents an artifact in both image quantification and dose estimation that arises when the target structure is smaller than the spatial resolution of the nuclear imaging system or the computational grid used for dose calculation, as illustrated in Figure 5.6. This effect is described by the relationship between the measured signal (M) and the true signal (T), which is blurred by the system's point spread function (PSF), as expressed in Equation 5-4. The objective of partial volume correction is to recover the true activity distribution T by applying the inverse of the known PSF. The PSF induced blurring results primarily from photon scatter, collimator penetration, and limited system resolution.

$$M = T \times PSF \qquad \text{Equation 5-4}$$

The measured signal for that voxel is an average of all enclosed tissues. This averaging process leads to a blurring of tissue interfaces and, critically, an underestimation of the true physical dose delivered to the small, dense tumor structure.

Uncorrected PVE introduces a systematic error in dose calculation, potentially leading to lower than intended dose delivery to the tumor, compromising Tumor Control Probability (TCP).

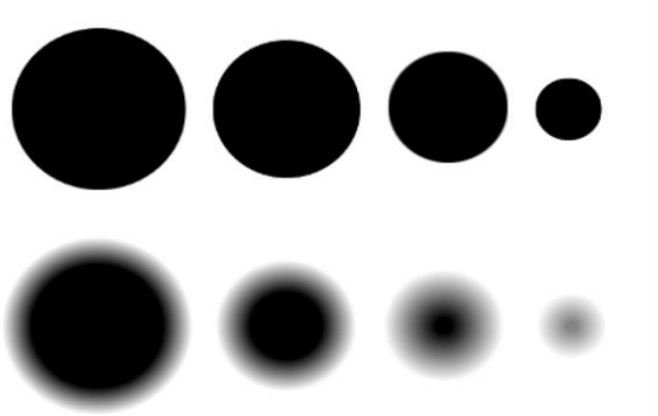

Figure 5.6: Illustration of PVE in reconstructed images of sphere phantoms. Top row: Represents the actual dimensions and sharp boundaries of the spheres. Bottom row: Shows the blurring and signal loss due to PVE after image reconstruction, particularly evident in small tumor.

For example, consider a lesion with a (T) of 50 kBq mL^{-1}. After reconstruction, the (M) decreases to 35 kBq mL^{-1} due to PSF induced blurring.

b) Applying Partial Volume Correction (PVC)

PVC is applied to compensate for PVE-related losses and restore the true activity distribution. This can be achieved by deconvolving the PSF or using empirically derived Recovery Coefficients (RCs) obtained from phantom calibration studies.

$$T_{estimated} = \frac{M}{Rc} \qquad \text{Equation 5-5}$$

If the RC for a 10 mL sphere is 0.70, then by using Equation 5-5:

$$T_{estimated} = \frac{35}{0.70} = 50 \text{ kBq mL}^{-1}$$

PVC effectively improves quantitative accuracy in image-based dosimetry by compensating for spatial resolution losses. The corrected activity values enhance the reliability of AD estimates, particularly for small lesions or heterogeneous activity distributions.

5.2.4 Partition Model (Multi-Compartment)

The Partition Model is the preferred and more accurate method for Yttrium 90 (Y-90 SIRT) dosimetry. It's an advanced approach that recognizes the non-uniform distribution of microspheres in the liver.

Instead of treating the entire liver lobe as a single unit, this model partitions the total radiation activity and AD among specific biological regions (or compartments).

Table 5.6: Summary of dosimetric compartments and their clinical roles in Y-90 SIRT.

Compartment	Purpose	Clinical Significance
Tumor	To calculate the maximum therapeutic dose	Determines if the treatment is likely to be effective
Normal Liver	To calculate the dose to healthy tissue	Crucial for ensuring the dose is below the threshold for radiation-induced liver disease (usually less than 50 Gy)
Lungs	To account for hepatic-pulmonary shunting	Ensures the lung dose is below the critical safety limit (usually less than 30 Gy)

This model is individualized using quantitative data derived from the pre-treatment Technetium-99m Macroaggregated Albumin (Tc-99m MAA) SPECT/CT scan.

The following parameters are applied;

1) **Tumor-to-Normal Uptake Ratio (TNR)**: Represents the ratio of activity concentration in the tumor relative to the surrounding normal liver tissue.

$$TNR = \frac{C_T / M_T}{C_N / M_N} \qquad \text{Equation 5-6}$$

2) **Lung Shunt Fraction (LSF)**: Indicates the proportion of microspheres expected to reach the lungs.

$$LSF = \frac{\text{Lung counts}}{\text{Lung counts} + \text{Liver counts}} \times 100 \qquad \text{Equation 5-7}$$

3) **Fraction of Hepatic Activity to Tumor (FT)**: Determined from Tc-99m MAA SPECT/CT using the tumor mass M_T (kg), perfused normal-liver massM_N (kg), and TNR.

$$F_T = \frac{TNR \times M_T}{TNR \times M_T + M_N} \qquad \text{Equation 5-8}$$

4) **Fraction of Hepatic Activity to Normal Liver (FN):** Derived from the same dataset, representing the remaining hepatic activity not localized in the tumor.

$$F_N = 1 - F_T \qquad \text{Equation 5-9}$$

5) **Compartment Dose Calculations:** ADs are computed using the Y-90 dose conversion factor 49.7 Gy kg GBq^{-1}.

$$D_T = 49.7 \times \frac{A_o - (1 - LSF)F_T}{M_T} \qquad \text{Equation 5-10}$$

$$D_N = 49.7 \times \frac{A_o - (1 - LSF)F_N}{M_N} \qquad \text{Equation 5-11}$$

$$D_L = 49.7 \times \frac{A_o LSF}{M_L} \qquad \text{Equation 5-12}$$

Where A_o refer to administered activity (GBq), M_T,M_N,$M_L$refer as tumor, normal-liver, and lung masses (kg), LSF refers to lung shunt fraction (%), FT, FN refers to fractions of hepatic activity in tumors and normal liver respectively.

The partition model is gold standard because it allows the clinician to maximize the therapeutic dose to the tumor while strictly limiting the dose to the healthy liver parenchyma and lungs, leading to safer and potentially more effective treatment.

5.3 Consideration for Heterogeneous Dose Distribution

MRT often results in non-uniform dose distributions within organs and tumors due to variable radiopharmaceutical uptake. Understanding and accounting for this heterogeneity is crucial for accurately predicting both therapeutic effects and potential toxicities.

Voxel-based dosimetry calculates the AD on a fine 3D grid, allowing visualization of spatial dose variations at the sub-organ level. This approach provides detailed 3D dose maps that reflect true heterogeneity, enabling more personalized treatment evaluation.

Dose Volume Histogram (DVH) analysis summarizes how dose is distributed across a volume by plotting the percentage of volume receiving a specific dose.

It is an essential tool to quantify heterogeneity and guide dose constraints for both tumor control and organ-at-risk protection.

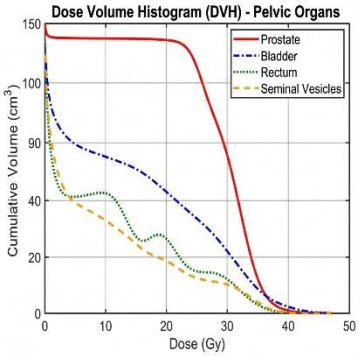

Figure 5.7: Dose Volume Histogram (DVH) comparing dose distributions across different pelvic organs. The graph illustrates the cumulative volume (cm^3) of the prostate, bladder, rectum, and seminal vesicles receiving varying radiation doses. The prostate (red curve) receives the highest dose coverage, while the bladder, rectum, and seminal vesicles receive lower and more variable dose distributions, highlighting organ-specific exposure and potential risk areas. (Image generated using artificial intelligence)

Radiobiological models such as Normal Tissue Complication Probability (NTCP) and Tumor Control Probability (TCP) incorporate dose heterogeneity to estimate clinical outcomes. These models are more predictive than mean dose alone because they account for variations in dose-response across tissues.

Table 5.7: Comparison of tumor control probability (TCP) and normal tissue complication probability (NTCP).

Aspect	**Tumor Control Probability (TCP)**	**Normal Tissue Complication Probability (NTCP)**
Definition	• The probability of complete tumor eradication in molecular radiotherapy remains low, except in selected settings such as I-131 therapy for thyroid carcinoma	• Probability of causing a clinically significant complication in normal tissue from radiation exposure
Objective	• to slow tumor progression	• Minimize radiation-induced toxicity
Mathematical Models	• Poisson statistics, Linear-Quadratic (LQ) model	• Lyman-Kutcher-Burman (LKB), Sigmoid dose-response
Dose-Response Curve	• Sigmoidal – increasing dose improves control up to a plateau	• Sigmoidal – increasing dose increases risk of complication
Key Parameters	• Tumor radiosensitivity (α/β), Clonogenic cell number, Dose per fraction and total dose	• Tissue-specific α/β, Volume effect (n), TD50 (dose causing 50% complication)

Dependence on Volume	• Less dependent on volume (for uniform tumors)	• Highly dependent on irradiated volume (serial vs. parallel organs)
Clinical Relevance	• Guides dose escalation to achieve better tumor control	• Informs organ dose limits to avoid side effects
Common Use	• Planning target volume (PTV) dose prescription	• Setting dose constraints to organs at risk (OARs)
Example Application	• Evaluating whether a prescribed dose will control prostate cancer	• Estimating risk of pneumonitis from lung radiation in thoracic RT

High-resolution quantitative imaging techniques like SPECT/CT and PET/CT are used to capture spatial variations in radiotracer uptake. These images provide the input data necessary for voxel-based dosimetry and radiobiological modelling, enhancing the accuracy of heterogeneous dose assessment.

Regions within the tumor that receive sub-therapeutic doses may lead to treatment failure, while hotspots in normal tissues may cause unexpected toxicity. Recognizing and quantifying these dose variations is key to optimizing treatment planning and balancing efficacy with safety.

Table 5.8: AD response recommendations for malignancies.

Tumor Type	Key Outcome	Optimal Tumor AD (Gy)	References
Thyroid Metastases	• Increased elimination	• > 80	(Maxon et al., 1992)
Hepatocellular (HCC)	• Increased survival (OS)	• > 200	(Hermann et al., 2020)
Neuroendocrine (NET)	• Higher probability of response	➢ 10 (per cycle) or • > 60 (cumulative exceeding dose)	(Ilhan et al., 2017)
mCRPC (Prostate)	• PSA decline	• > 10 (per cycle)	(Violet et al., 2019)

5.4 References

Beauregard, J. M., Hofman, M. S., Pereira, J. M., Eu, P., & Hicks, R. J. (2011). Quantitative (177Lu) SPECT (QSPECT) imaging using a commercially available SPECT/CT system. *Cancer Imaging, 11*(1), 56–66.

Bolch, W. E., Eckerman, K. F., Sgouros, G., & Thomas, S. R. (2009). MIRD pamphlet no. 21: A generalized schema for radiopharmaceutical dosimetry—Standardization of nomenclature. *Journal of Nuclear Medicine, 50*(3), 477–484.

Del Prete, M., Buteau, F. A., Arsenault, F., et al. (2012). Dosimetry in peptide receptor radionuclide therapy: A review. *Nuclear Medicine Communications, 33*(11), 1209–1215.

Dewaraja, Y. K., Frey, E. C., Sgouros, G., et al. (2012). MIRD pamphlet no. 23: Quantitative SPECT for patient-specific 3-dimensional dosimetry in internal radionuclide therapy. *Journal of Nuclear Medicine, 53*(8), 1310–1325.

Ferrer, L., Kraeber-Bodéré, F., Bodet-Milin, C., et al. (2010). Three-dimensional dosimetry in targeted radionuclide therapy: Techniques and limitations. *Cancer Biotherapy and Radiopharmaceuticals, 25*(2), 221–230.

Gear, J. I., Cox, M. G., Esser, J., et al. (2013). The use of PET/CT for 3D dose estimation in radionuclide therapy. *Physics in Medicine & Biology, 58*(12), 4233–4250.

Grimes, J., & Celler, A. (2014). Comparison of internal dosimetry estimates obtained using organ-level, voxel S value, and Monte Carlo techniques. *Medical Physics, 41*(9), 092501.

Hänscheid, H., Lapa, C., Buck, A. K., Lassmann, M., & Werner, R. A. (2018). Dose mapping after endoradiotherapy with 177Lu-DOTATATE/DOTATOC by a single measurement after 4 days. *Journal of Nuclear Medicine, 59*(1), 75–81.

Haste, P., Brill, A. B., & Zanzonico, P. B. (2020). Voxel-level dosimetry: From MIRD to the clinic. *Medical Physics, 47*(6), e66–e84.

Hindorf, C., Glatting, G., Chiesa, C., Linden, O., & Flux, G. (2010). EANM Dosimetry Committee guidelines for bone marrow and whole-body dosimetry. *European Journal of Nuclear Medicine and Molecular Imaging, 37*(6), 1238–1250.

Hobbs, R. F., & Sgouros, G. (2009). The role of dosimetry in 131I therapy of thyroid cancer. *Journal of Nuclear Medicine, 50*(4), 499–502.

Hobbs, R. F., Song, H., Watchman, C. J., Bolch, W. E., et al. (2013). A time-dependent modeling approach to predict tumor control probability after radiopharmaceutical therapy. *Medical Physics, 40*(10), 102503.

Ljungberg, M., et al. (2011). SPECT/CT: Applications in internal radionuclide dosimetry. *Quarterly Journal of Nuclear Medicine and Molecular Imaging, 55*(1), 10–22.

Ritt, P., Vija, A. H., Hornegger, J., & Kuwert, T. (2011). Absolute quantification in SPECT. *European Journal of Nuclear Medicine and Molecular Imaging, 38*(Suppl 1), S69–S77.

Sgouros, G. (2005). Dosimetry of internal emitters. *Journal of Nuclear Medicine, 46*(Suppl 1), 18S–27S.

Sgouros, G. (2008). Accounting for tumor and normal tissue heterogeneity in dosimetry. *Seminars in Nuclear Medicine, 38*(4), 321–334.

Sgouros, G., Howell, R. W., Bolch, W. E., Fisher, D. R., et al. (2010). MIRD pamphlet no. 22: Radiobiology and dosimetry of alpha-particle emitters for targeted radionuclide therapy. *Journal of Nuclear Medicine, 51*(2), 311–328.

Stabin, M. G., Sparks, R. B., & Crowe, E. (2005). OLINDA/EXM: The second-generation personal computer software for internal dose assessment in nuclear medicine. *Journal of Nuclear Medicine, 46*(6), 1023–1027.

Violet, J., Jackson, P., Ferdinandus, J., et al. (2019). Dosimetry of 177Lu-PSMA-617 in metastatic castration-resistant prostate cancer: Correlations between pretherapeutic imaging and whole-body tumor dose and treatment outcomes. *Journal of Nuclear Medicine, 60*(4), 517–523.

CHAPTER 6

SAMPLE CASE STUDY IN INTERNAL DOSIMETRY

This chapter presents practical examples illustrating how internal dosimetry principles are applied to different therapeutic radionuclides such as I-131 NaI, Lu-177 DOTATATE, and Y-90 SIRT each representing a major clinical application in MRT. The aim is to demonstrate the workflow from image acquisition to AD estimation and interpretation, highlighting how differences in radiopharmaceutical kinetics, emission characteristics, and biophysical distribution influence dosimetric calculations.

6.1 Pre-MRT Dosimetry of I-131 NaI for the Treatment of Differentiated Thyroid Cancer (DTC)

A 61-year-old male diagnosed with widely invasive Follicular Thyroid Carcinoma underwent total thyroidectomy, with histopathological confirmation of differentiated thyroid carcinoma (DTC). The patient received a prescribed activity of 201 MBq of I-131. Whole-body planar imaging and SPECT/CT scans were acquired at 1, 24, 48, and 72 hours after I-131 administration, with an optional acquisition at 96 hours. Approximately 2 mL of whole blood was collected at 2-, 24-, 48-, and 72-hour post-administration. Using data summarized in Table 6.1 and Table 6.2, determine the optimal therapeutic activity of I-131 that achieves a curative effect while maintaining acceptable toxicity levels.

Table 6.1: I-131 uptake for whole-body (%).

Time (h)	WB_{net} (counts)	Normalized counts (%)
1.48	1277437	100
23.98	471469	36.9
48.02	241458	18.9
72.07	155404	12.2

Table 6.2: I-131 uptake in the blood (%).

Time (h)	Activity concentration of blood (Bq ml^{-1})	Normalized counts (%)
3.45	3357.74	100
23.90	1555.56	46.3
48.05	964.12	28.7
72.08	528.51	15.7

The activity prescribed to the patient is decided after reviewing the calculation of radiation exposure to the organ at risk such as bone marrow and lung together to ensure the treatment is effective.

6.1.1 Steps and Solutions

Procedure for estimating the Mean AD to the OAR

a) Determine the blood percentage uptake of I-131 in the OAR at each imaging time point.

b) Calculate the $\tilde{A}$ for 1 ml blood.

c) Estimate the AD delivered to the target OAR is the bone marrow with blood as surrogate using the calculated $\tilde{A}$ and appropriate dosimetric models.

6.1.2 Detail procedure

c) Procedure for Determining OAR Percentage Uptake of I-131 NaI at Each Time Point.

The primary source organs for I-131-NaI are blood (surrogate red marrow) and whole body.

i. The mean AD to the blood per unit administered activity was calculated by adding the self-irradiation of the blood and the radiation contribution from the whole body, using the following formula.

$$\frac{\bar{D}_{blood}}{A_o}\left[\frac{mGy}{MBq}\right] = 108 \times \tau_{mL\ of\ blood}[h] + \frac{0.0188}{(wt[kg])^{2/3}} \times \tau_{total\ body}[h] \qquad \text{Equation 6-1}$$

Where $\tau_{mL\ of\ blood}$ refer to blood $\tilde{A}$ and $\tau_{total\ body}$ refer to wholebody $\tilde{A}$.

ii. The blood and lung are designated as the OAR and serves as the primary target for dose estimation.

iii. To determine the percentage uptake of I-131 in the OAR at each imaging time point using data from Table 6.1 and Table 6.2, the following formula was applied, and the results are presented in Table 6.3.

iv. Percentage Uptake $= \frac{A_t}{A_o} \times 100.$

Where A_t refers to the activity measured at time t and A_o are initial administered activity.

Table 6.3: Comparative I-131 uptake in blood and whole body at different time points.

Time (h)	Blood uptake (%)	Whole Body uptake (%)
1.48	100	8.54
23.98	36.91	3.95
48.02	18.90	2.45
72.07	12.17	1.34

d) Procedure for Estimating the $\tilde{A}$ for Blood and Whole Body.

i. Compute the $\tilde{A}$ for blood and whole body using the OLINDA software, as illustrated in **APPENDIX A**.

ii. Table 6.1 and Table 6.2 show that the $\tilde{A}$ for the whole-body uptake, calculated using the OLINDA disintegration calculator, was 34.1 hours, while the corresponding $\tilde{A}$ for the red marrow determined by the same tool was 3.31 hours.

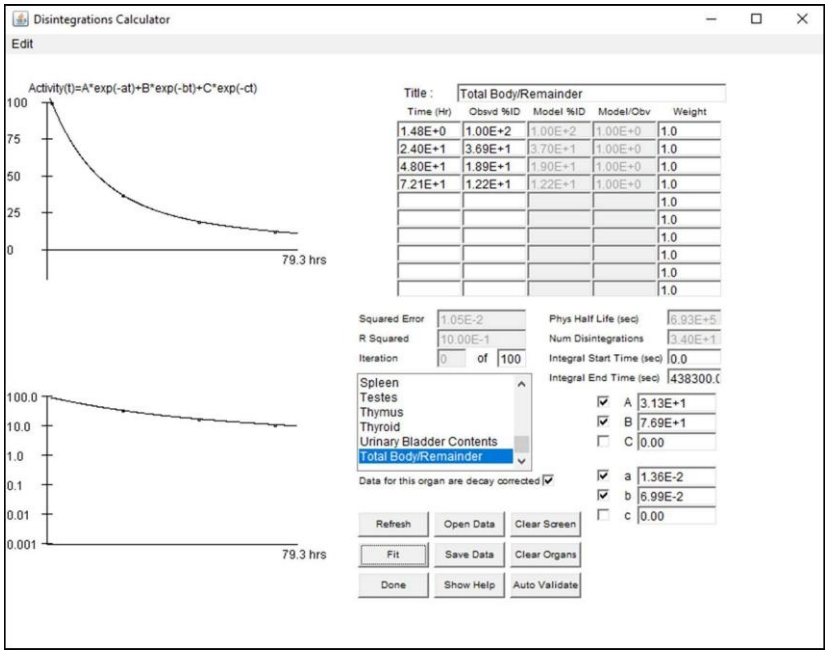

Figure 6.1: The $\tilde{A}$ for the whole-body activity based on OLINDA disintegration calculator was 34.1 hours.

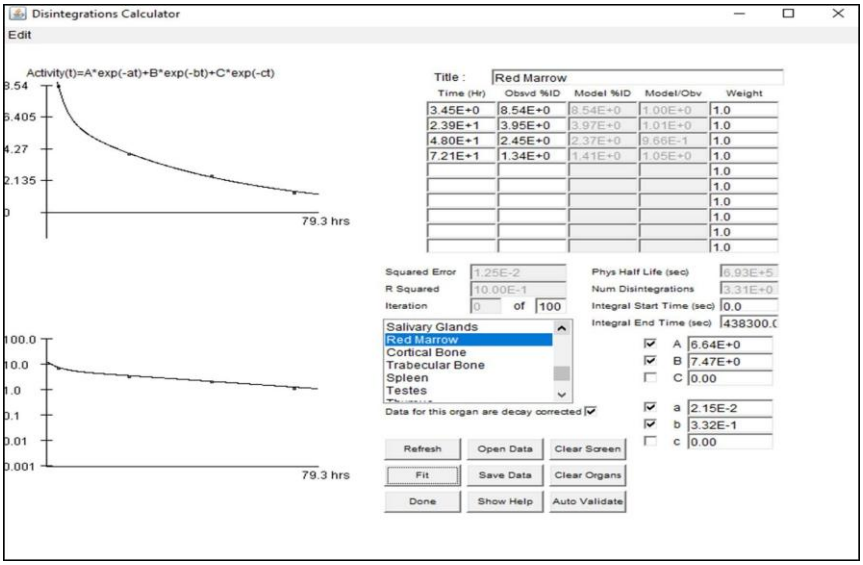

Figure 6.2: The $\tilde{A}$ for red marrow based on OLINDA disintegration calculator was 3.31 hours.

iii. Critical lung activity based on 48 hours whole-body retention time was 18.9 %. Based on the Benua criterion, the maximum permissible retained activity is 2.96 GBq. By using Equation 6-2.

$$A_{max} \times 0.189 = 2.96 \text{ GBq} = \frac{2.96}{0.189} = 15.66 \text{ GBq} \qquad \text{Equation 6-2}$$

iv. Thus, the calculated maximum administrable activity is 15.66 GBq.

e) Estimate the AD delivered to the target OAR using the calculated $\tilde{A}$ and appropriate dosimetric models.

i. The activity to be administered to achieve a target AD of 2 Gy to the blood was calculated using the following equation

$$A_{adm}[\text{GBq}] = \frac{2}{\bar{D}\left[\frac{\text{Gy}}{\text{GBq}}\right]} \qquad \text{Equation 6-3}$$

ii. Based on Equation 6-3, the critical blood activity (CBA) for this patient was 19.3 GBq.

iii. Based on the dosimetry result, maximum I-131 activity safe to administered is 15.66 GBq.

6.2 Y-90 microspheres for the treatment of primary and metastatic liver cancer

A 63-year-old male presented with right upper quadrant discomfort and mild weight loss over three months. Liver function tests were within normal limits, and alpha-fetoprotein (AFP) was elevated at 450 ng mL^{-1}. Contrast-enhanced MRI revealed a 5 cm hypervascular lesion in segment VIII of the liver, consistent with segmental hepatocellular carcinoma (HCC), with no evidence of portal vein thrombosis or extrahepatic spread. The patient had no history of cirrhosis or hepatitis B/C infection, and the Child–Pugh score was A5, indicating preserved liver function.

Following multidisciplinary tumor board discussion, the patient was deemed unsuitable for surgical resection due to limited hepatic reserve but was considered an ideal candidate for locoregional therapy. Tc-99m macroaggregated albumin (MAA) simulation demonstrated a pulmonary shunt fraction of 8%, meeting eligibility for Yttrium-90 using resin microspheres.

The procedure was planned for the right hepatic artery, with coil embolization of the gastroduodenal artery performed during mapping to prevent non-target radiation.

The lung mass (M_L) follows ICRP 89 values of 1200 g for the adult male and 950 g for the adult female, giving an average of about 1000 g per lung, or it can be derived from patient-specific CT using a tissue density of (ρ = 0.25 gm L^{-1}), where ICRP 89 reports a density of 1.05 g mL^{-1} for air-free lung tissue filled with blood and an average in vivo lung density of about 0.25 g mL^{-1} when air is present. Inputs obtained from MAA SPECT/CT include a lung shunt fraction (LSF) of 0.08, a tumor volume of 65 mL corresponding to a tumor mass (M_T) of 0.067 kg, a perfused normal-liver volume of 1100 mL corresponding to a normal-liver mass (M_N) of 1.133 kg, and a tumor-to-normal uptake ratio (TNR) of 3.2.

6.2.1 Steps and Solutions

Procedure for estimating the Mean AD to the OAR

a) Assess the lung shunt fraction using Tc-99m MAA scintigraphy and ensure it is below 10% for safety.

b) Calculate the required Y-90 activity using the partition.

c) Administer Y-90 microspheres through selective catheterization of the hepatic artery feeding the tumor.

d) Acquire Y-90 PET/CT or Bremsstrahlung imaging to verify microsphere distribution after treatment.

6.2.2 Detail procedure

a) Assess the lung shunt fraction (LSF) using Tc-99m MAA scintigraphy and ensure it is below 10%.

i. The lung shunt fraction (LSF) was measured using Tc-99m MAA planar scintigraphy and determined to be 8%, remaining below the 10% safety threshold defined in Equation 5-7.

b) Calculate the required Y-90 SIRT activity using the partition model

i. Using Equation 5-8 and Equation 5-9, the intrahepatic activity fractions were derived as $F_T = 0.159$ and $F_N = 0.841$.

ii. By apply Equation 5-10 until Equation 5-12, the Dose goals and limits (resin): target tumor dose $D_T^{goal} = 120$ Gy; normal liver limit $D_N^{max} = 70$ Gy; lung limit $D_L^{max} = 30$ Gy/session; lung mass $M_L = 1.0$ kg, the calculated activities were $A_oT = 1.11$ GBq, $A_oN = 2.06$ GBq, $A_oN = 7.55$ GBq.

iii. Thus, $A_o = 1.11$ GBq is the optimal therapeutic activity to be delivered for effective and safe Y-90 treatment in this case.

6.3 Lu-177 DOTATATE for the Treatment of Neuroendocrine Tumors

A 55-year-old female with a well-differentiated midgut neuroendocrine tumor and liver-dominant metastases showed disease progression despite prior treatments, including ileal tumor resection, platinum-based chemotherapy, and somatostatin analog therapy. Functional imaging with Ga-68 DOTATATE PET/CT confirmed high somatostatin receptor expression, prompting initiation of Lu-177 DOTATATE peptide receptor radionuclide therapy (PRRT). The first cycle involved administration of 7.4 GBq (200 mCi) via 30-minute intravenous infusion with amino acid nephroprotection, with three additional cycles planned at 8-week intervals.

The primary aim of post-therapy dosimetry was to evaluate the absorbed radiation doses delivered to tumors and critical organs, with particular focus on

the kidneys. Quantitative SPECT/CT imaging was performed at five time points following radiopharmaceutical infusion: 4, 24, 48, 72, and 168 hours as shown in Figure 6.3.

Whole-body and abdominal SPECT/CT acquisitions were conducted, incorporating CT-based attenuation and scatter corrections to ensure accurate quantification of radiotracer activity.

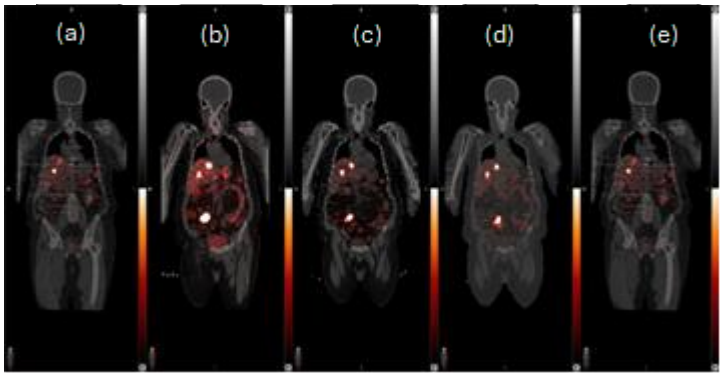

Figure 6.3: Five time point Lu-177 DOTATATE serial scan. (a) 4 h, (b) 24 h, (c) 48 h, (d) 72 h and (e) 168 h.

The AD to the OAR (kidneys) and to the tumor 1 (D_{T1}) located at the lymph node were calculated based on the data provided in Table 6.1 and Table 6.2.

6.3.1 Steps and Solutions

a) Determine the percentage uptake of Lu-177 DOTATATE in the organ at each imaging time point.

b) Calculate the $\tilde{A}$ for all relevant organs.

c) Estimate the AD delivered to the target organ using the calculated $\tilde{A}$ and appropriate dosimetric models.

6.3.2 Detail of the procedure

a) Procedure for Determining Percentage Uptake of Lu-177 DOTATATE OAR at Each Imaging Time Point.

i. The primary source organs for Lu-177 DOTATATE include the kidneys, liver, spleen, and whole body.

ii. The kidneys are designated as the OAR and serves as the primary target for dose estimation.

iii. Tumor dosimetry calculations are based on a self-irradiation (self-dose) model.

iv. To estimate theÃ, the measured activity from the SPECT workstation should be normalized to the administered activity, as outlined in Table 6.6.

Table 6.4: Organ uptake (MBq) for Lu-177 DOTATATE from Figure 6.3.

Time (h)	Kidneys	Liver	Spleen	Whole body
4.38	147	74	15	7252
24.02	161	1184	629	4743
48.10	102	1110	1110	2427
72.05	56	111	259	1894
168.18	5	2	44	1295

Table 6.5: Tumors physical character and uptake (%).

Time (h)	Tumor 1
2.38	0.00
4.02	1.04
20.22	0.86
48.05	0.49
94.18	0.22
Volume (mL)	10
Mass (g)	10.30

b) Procedure for Estimating the $\tilde{A}$ for Relevant Organs

i. Estimate the organ uptake (%) for Lu-177 DOTATATE by dividing the measured organ activity at time T by the total injected activity.

ii. Compute the $\tilde{A}$ for the kidneys using the OLINDA software, following the procedure described in Appendix A.

iii. The calculated organ uptake and corresponding $\tilde{A}$ values are summarized in Table 6.6 and Table 6.7, as obtained from the OLINDA output.

Table 6.6: Organ Uptake (%) Lu-177 DOTATATE.

Time (h)	Kidneys	Liver	Spleen	Whole body
4.38	1.99	1.00	0.20	98.00
24.02	2.18	16.00	8.50	64.09
48.10	1.38	15.00	15.00	32.80
72.05	0.76	1.50	3.50	25.59
168.18	0.07	0.03	0.59	17.50

Table 6.7: The TIAC result results derived from bi-exponential fitting for major organs and whole body.

Organ	Kidneys	Liver	Spleen	Whole body
TIAC, $\frac{\tilde{A}}{A_0}$ (h)	1.25	7.6	6.79	41.6

Table 6.8: AD according to the ORNL of adult computational phantoms (mGy).

Target Organ	Alpha	Beta	Photon	Total
Adrenals	0.00E+00	3.55E+02	9.18E+01	4.46E+02
Brain	0.00E+00	3.55E+02	2.83E+01	3.83E+02
Breasts	0.00E+00	3.55E+02	2.73E+01	3.82E+02
Gallbladder Wall	0.00E+00	3.55E+02	9.59E+01	4.51E+02
LLI Wall	0.00E+00	3.55E+02	4.73E+01	4.02E+02
Small Intestine	0.00E+00	3.55E+02	5.72E+01	4.12E+02
Stomach Wall	0.00E+00	3.55E+02	8.64E+01	4.41E+02
ULI Wall	0.00E+00	3.55E+02	5.92E+01	4.14E+02
Heart Wall	0.00E+00	3.55E+02	5.97E+01	4.14E+02
Kidneys	**0.00E+00**	**3.14E+03**	**1.41E+02**	**3.28E+03**
Liver	0.00E+00	2.50E+03	1.34E+02	2.63E+03
Lungs	0.00E+00	3.55E+02	5.25E+01	4.07E+02
Muscle	0.00E+00	3.55E+02	4.06E+01	3.95E+02
Ovaries	0.00E+00	3.55E+02	5.07E+01	4.05E+02
Pancreas	0.00E+00	3.55E+02	1.33E+02	4.87E+02
Red Marrow	0.00E+00	2.62E+02	4.41E+01	3.07E+02

Osteogenic Cells	0.00E+00	1.14E+03	7.63E+01	1.22E+03
Skin	0.00E+00	3.55E+02	2.27E+01	3.77E+02
Spleen	0.00E+00	2.33E+04	4.97E+02	2.38E+04
Testes	0.00E+00	3.55E+02	3.08E+01	3.85E+02
Thymus	0.00E+00	3.55E+02	3.98E+01	3.94E+02
Thyroid	0.00E+00	3.55E+02	3.65E+01	3.91E+02
Urinary Bladder Wall	0.00E+00	3.55E+02	4.36E+01	3.98E+02
Uterus	0.00E+00	3.55E+02	5.05E+01	4.05E+02

Kidneys AD = 3.30 Gy.

c) Procedure for Estimating Tumor AD in Lu-177 DOTATATE Therapy.

i. Open the **OLINDA/EXM** software to initiate the dosimetry workflow as outlined in **APPENDIX A.**

ii. Proceed with steps (a) to (e), then record the sphere mass and AD data as show (Figure 9) at **APPENDIX A** into the spreadsheet to construct the graph. Apply an exponential fit function to perform the curve fitting within the graph.

iii. The fitted curve follows the relationship described by Equation 6-4, and the corresponding graph is presented in Figure 6.4 is used to determine the tumor AD.

$$AD = A \times m^{-a} \qquad \text{Equation 6-4}$$

Where A is fitting constant derived from regression analysis, M is referred to tumor mass, a is fitted exponent describing the mass dose relationship.

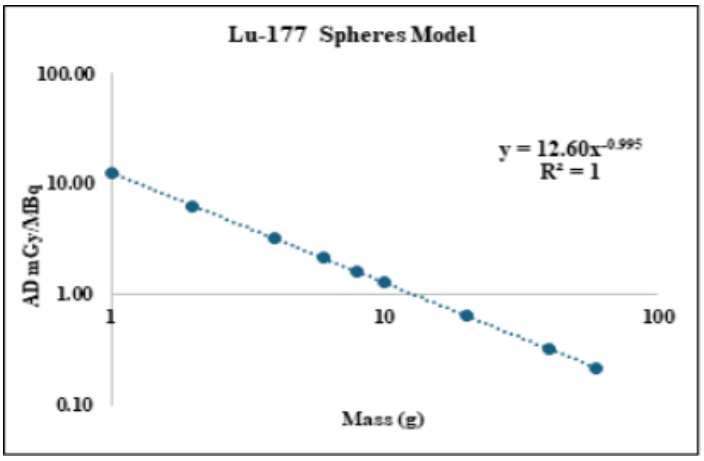

Figure 6.4: Lu-177 sphere self-ADs fit from Table 6.5.

iv. To accurately estimate the tumor AD, it is essential to convert tumor volume into tumor mass. The densities of tumor and bones vary, with tumor densities ranging from 1.03 to 1.05 g cm^{-3}.

v. The calculation of mean AD tumor is based on the Equation 6-4, where A and a are derived from the least square analysis fitting, while *y*-axis represents the D in mGy MBq^{-1} or Gy GBq^{-1} and x-axis represents the mass in grams.

vi. For example, in the case of D_{T1}, with a density of 1.03 g cm^{-3}, the mass is calculated to be 10.30 g. Substituting this mass into the Equation 6-5 gives

$$D_{T1} = 12.60 \times (10.30^{-0.995}) = 1.24 \text{ mGy MBq}^{-1} \quad \text{Equation 6-5}$$

vii. Given a dose of 7.4 GBq, D_{T1} is 1.24 Gy GBq^{-1} × 7.4 GBq

AD for D_{T1} = 9.18 Gy

CHAPTER 7

CORRELATION BETWEEN INTERNAL DOSIMETRY AND STANDARD UPTAKE VALUE

A key challenge in personalized MRT is linking imaging metrics, such as the Standard Uptake Value (SUV), to the AD in organs and tumors. SUV is widely used in PET (and quantitative SPECT) imaging as a measure of radiotracer uptake, and it serves as a proxy for activity concentration within a region. By understanding the correlation between SUV-based uptake measurements and internal dosimetry calculations, medical physicists can better predict dose distributions from diagnostic scans and optimize MRT. Real-world clinical applications and case studies are included to illustrate how SUV measurements inform or predict internal dose, along with challenges and discrepancies that can arise due to kinetic differences, imaging resolution limits, and biological variability.

7.1 Understanding SUV in Nuclear Medicine Imaging

SUV is a dimensionless quantity defined as the radioactivity concentration in a tissue region of interest divided by the injected activity normalized to patient body weight. In formula terms;

$$SUV = \frac{\text{Activity Concentration in tissue } \left(\frac{kBq}{ml}\right)}{\text{Activity concentration in whole body } \left(\frac{kBq}{g}\right)} \qquad \text{Equation 7-1}$$

where 1 mL of tissue is assumed to be approximately equivalent to 1 g in mass. This assumption simplifies the computation and supports the use of SUV as a standardized, unitless measure in quantitative imaging analysis.

This essentially compares the local concentration of radiotracer to an average concentration if the dose were uniformly distributed throughout the body. A higher SUV means greater uptake in that tissue relative to the rest of the body, appearing as a “hotter” region on the scan. SUV was originally popularized in PET (e.g. with F-18 FDG) but can be applied to SPECT imaging as well, provided the SPECT system is quantitatively calibrated. If the injected activity and patient’s weight are known, an SUV can be converted to activity per volume (e.g. Bq mL^{-1}) in the tissue. Modern SPECT/CT systems can report SUV values after proper

attenuation, scatter, and resolution corrections, analogous to PET SUV measurements.

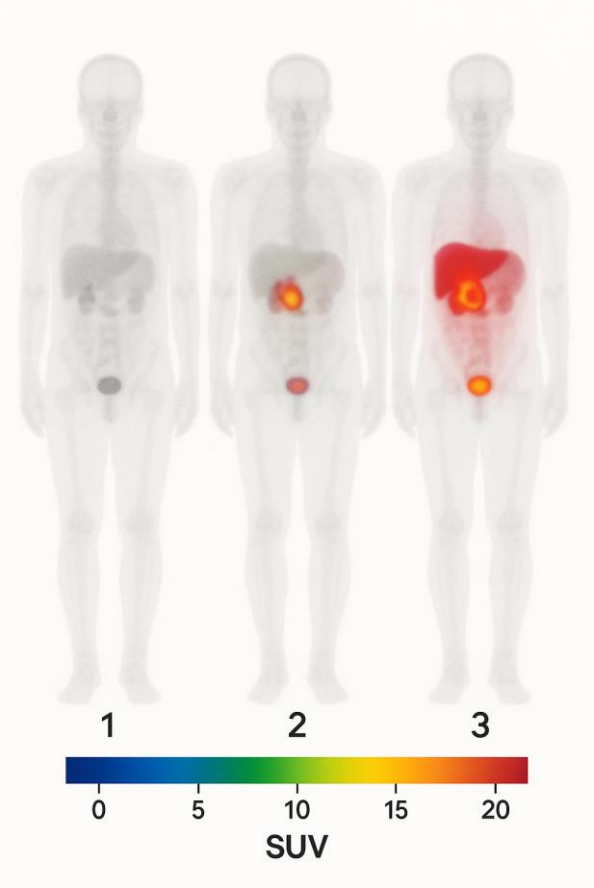

Figure 7.1: Illustration of SUV scale ranging.

Crucially for dosimetry, SUV provides a bridge to estimate absolute activity concentration from imaging. This makes SUV a convenient index: it is easily computed on scanners and reflects how much radiopharmaceutical is localized in a tissue at the time of imaging. In therapy planning, one might use an SUV from a diagnostic scan as a surrogate for how much activity a tumor or organ might accumulate.

For example, in Ga-68 DOTATATE PET imaging, a tumor showing an SUV of 10 indicates an uptake ten times greater per gram than the average whole-body activity. In principle, this suggests a potentially higher AD if a therapeutic radionuclide targeting the same molecular pathway is later administered.

SUV-based thresholds are sometimes applied in patient selection; tumors with very low SUVs are considered “cold” and may be less responsive to targeted MRT. For F-18 FDG, an SUV cut-off of 2.5 is commonly used to distinguish malignant from benign lesions. However, translating SUV values into AD estimates is complex and requires accurate quantitative calibration and

correction for time-dependent biodistribution, as discussed in the following sections.

As shown in Figure 7.2, MIRD schema represents an organ-level dosimetry approach based on predefined anatomical phantoms and reference biokinetic data. It assumes a uniform distribution of activity within each source organ and applies residence times together with S-values to calculate absorbed dose, resulting in mean organ or average tissue dose estimates. This approach is robust for whole-organ dose assessment and remains widely used for population-based dosimetry, regulatory reporting, and standard radiation risk evaluation. However, the assumption of uniform uptake limits its ability to resolve spatial heterogeneity, meaning that focal lesions, small structures, or intra-organ dose variations may not be adequately represented, potentially affecting interpretation of localized absorbed dose.

In contrast, the voxel-based method is a three-dimensional, tissue-level approach that uses patient-specific imaging data reconstructed into voxels. By preserving heterogeneous activity distributions within organs and lesions, it enables voxel-level absorbed dose calculations and generates personalized dose maps rather than organ averages. This method allows detailed characterization of intra-organ and intra-tumour variability and is particularly relevant for molecular radiotherapy, were spatial dose distribution influences treatment response and toxicity.

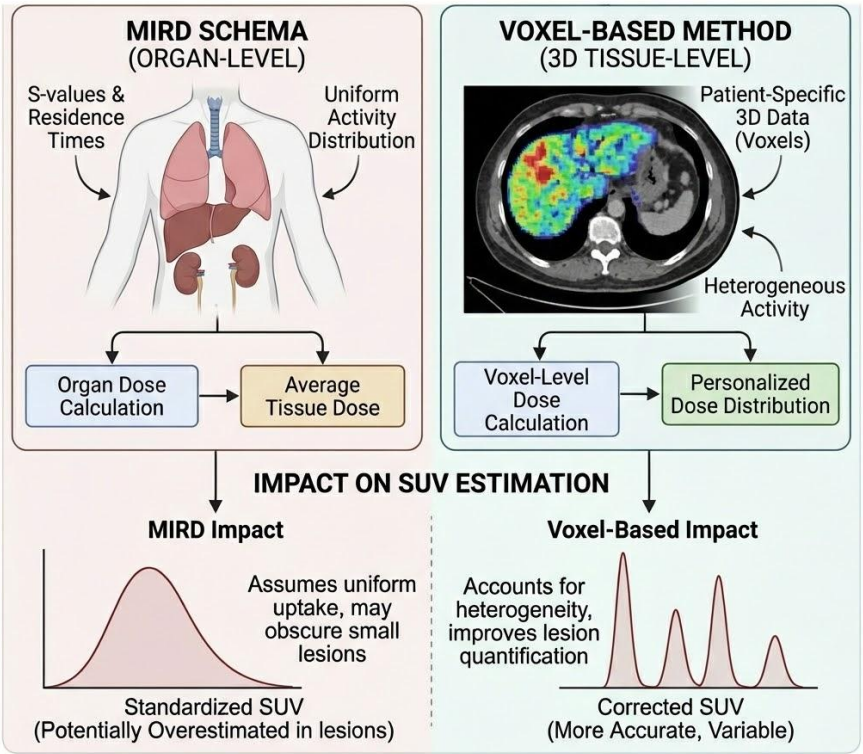

Figure 7.2: Comparison of internal dosimetry: MIRD Schema vs. Voxel-Based method and their impact on SUV estimation.

7.2 Types of Standardized Uptake Values (SUV) in Quantitative Imaging

The SUV is a quantitative parameter that reflects radiotracer uptake normalized to the administered activity and patient characteristics such as body weight or lean body mass. Various SUV metrics have been introduced to capture different aspects of tracer distribution and tumor metabolism. SUV_{MAX} represents the highest voxel value within a lesion and is widely used for its simplicity and reproducibility, although it can be affected by image noise and may overestimate activity in small or heterogeneous regions. SUV_{MEAN} refers to the mean uptake across the entire lesion, providing a measure of overall tracer distribution but depending heavily on accurate lesion delineation. SUV_{PEAK} is defined as the average SUV within a small, fixed spherical volume placed over the area of highest uptake. It offers a compromise between the noise sensitivity of SUV_{MAX} and the segmentation dependence of SUV_{MEAN}, making it suitable for multicentre studies where reproducibility is essential.

Beyond intensity-based metrics, volumetric parameters such as SUV_{MTV} (Metabolic Tumor Volume) and SUV_{TLG} (Total Lesion Glycolysis) extend the analysis to include tumor size and total metabolic activity. SUV_{MTV} quantifies the volume of metabolically active tumor tissue based on a predefined uptake threshold, integrating functional and morphological data to estimate total active burden. SUV_{TLG}, calculated as the product of SUV_{MEAN} and SUV_{MTV}, represents the total metabolic activity within the lesion and serves as a more comprehensive indicator of disease extent and response to therapy. Together, these SUV parameters provide complementary insights into tumor biology, enhancing the assessment of disease progression, treatment planning, and therapy monitoring in nuclear medicine and molecular imaging. All relevant information is summarized in Table 7.1, which consolidates the definitions, measurement bases, noise sensitivities, and interpretive significance of the different SUV parameters used in quantitative imaging.

Table 7.1: Summary of different Standardized Uptake Value (SUV) parameters, their definitions, measurement basis, sensitivity to image noise, and the biological or clinical aspect each reflects in quantitative nuclear imaging.

Parameter	Definition	Measurement Basis	Sensitivity to Noise	Reflects
SUV_{MAX}	Maximum voxel uptake	Single voxel	High	Peak uptake intensity
SUV_{MEAN}	Mean uptake in ROI	Entire tumor	Low	Global lesion activity
SUV_{PEAK}	Mean uptake in fixed small volume (1 cm^3)	Small high-uptake zone	Moderate	Localized activity robustness

SUV_{MTV}	Volume above threshold	3D tumor extent	Moderate	Metabolically active tumor volume
SUV_{TLG}	SUV_{MEAN} × MTV	Composite parameter	Moderate	Total metabolic burden

Each SUV type provides distinct quantitative insight. Combining them enables comprehensive evaluation of lesion intensity, volume, and total activity, essential for dosimetry, response monitoring, and prognostic analysis in MRT and molecular imaging.

SUV serves as a key bridge between nuclear medicine imaging and therapeutic dosimetry. The underlying principle indicates that SUV is proportional to activity concentration and, when time and energy are incorporated, it directly relates to AD. In clinical practice with radionuclides such as Lu-177, I-131, and Y-90, areas exhibiting high SUV often align with higher ADs, allowing imaging data to guide therapy planning.

However, this relationship is not absolute. Variability in pharmacokinetics, imaging accuracy, and individual patient physiology can affect the correlation. Medical physicists must consider these factors when interpreting SUV values in dosimetric analysis. Advancements in quantitative imaging, harmonization of SUV measurements across modalities including SPECT, and the integration of artificial intelligence are expected to strengthen the predictive value of SUV in internal dosimetry.

7.3 References

Bolch, W. E., Bouchet, L. G., Robertson, J. S., Wessels, B. W., Siegel, J. A., Howell, R. W., Erdi, A. K., Aydogan, B., Costes, S., Watson, E. E., Brill, A. B., Charkes, N. D., Fisher, D. R., Hays, M. T., & Thomas, S. R. (1999). MIRD pamphlet no. 17: The dosimetry of nonuniform activity distributions—Radionuclide S values at the voxel level. *Journal of Nuclear Medicine, 40*(1), 11S–36S.

Bolch, W. E., Eckerman, K. F., Sgouros, G., Thomas, S. R., Brill, A. B., Fisher, D. R., Howell, R. W., Meredith, R., & Wessels, B. W. (2009). MIRD pamphlet no. 21: A generalized schema for radiopharmaceutical dosimetry—Standardization of nomenclature. *Journal of Nuclear Medicine, 50*(3), 477–484.

Chaichana, A., & Tocharoenchai, C. (2016). Development of a software tool for internal dosimetry using the MIRD method. *Journal of Physics: Conference Series, 694*(1), 012056.

Dewaraja, Y. K., Frey, E. C., Sgouros, G., Brill, A. B., Roberson, P., Zanzonico, P. B., & Ljungberg, M. (2012). MIRD pamphlet no. 23: Quantitative SPECT for

patient-specific 3-dimensional dosimetry in internal radionuclide therapy. *Journal of Nuclear Medicine, 53*(8), 1310–1325.

Dewaraja, Y. K., Ljungberg, M., Green, A. J., Zanzonico, P. B., Frey, E. C., Bolch, W. E., Brill, A. B., Dunphy, M., Fisher, D. R., Howell, R. W., Meredith, R. F., Sgouros, G., & Wessels, B. W. (2013). MIRD pamphlet no. 24: Guidelines for quantitative 131I SPECT in dosimetry applications. *Journal of Nuclear Medicine, 54*(12), 2182–2188.

Ljungberg, M., Celler, A., Konijnenberg, M. W., Eckerman, K. F., Dewaraja, Y. K., & Sjögreen-Gleisner, K. (2016). MIRD pamphlet no. 26: Joint EANM/MIRD guidelines for quantitative 177Lu SPECT applied for dosimetry of radiopharmaceutical therapy. *Journal of Nuclear Medicine, 57*(1), 151–162.

CHAPTER 8

RADIATION PROTECTION FOR STAFF IN INTERNAL DOSIMETRY

Nuclear medicine therapies involve the administration of radiopharmaceuticals that emit ionizing radiation for therapeutic purposes. These agents, such as I-131, Lu-177 and Y-90, are used for treating conditions like thyroid cancer, neuroendocrine tumors, prostate cancer, and liver malignancies. Following administration, the patient becomes a temporary source of radiation, requiring strict radiation protection practices for staff members involved in dosimetry and patient care.

This chapter provides comprehensive guidance for nuclear medicine technologists, medical physicists, and nursing staff who engage in internal dosimetry procedures pre and post-therapy. The goal is to ensure that occupational exposures remain within prescribed regulatory limits, while still delivering effective patient care and accurate dosimetric assessments.

8.1 Radiation Protection Principles

The cornerstone of radiation safety is the application of the ALARA principle keeping radiation exposure *As Low As Reasonably Achievable*. This principle is achieved by optimizing three fundamental parameters:

8.1.1 Time

The amount of radiation exposure is directly proportional to the time spent near the source. Therefore, minimizing the time spent close to high-activity patients significantly reduces exposure. For example, procedures like blood sampling, image acquisition, or biodistribution assessments should be planned to be efficient and quick. Staff should rehearse steps, prepare all equipment in advance, and avoid unnecessary delays near the patient.

8.1.2 Distance

Radiation intensity decreases with the square of the distance from the source, according to the inverse square law. Staff should maintain as much distance as

possible from patients. Tools such as tongs, extended tubing, or remote video monitoring systems can help maintain physical separation during clinical tasks.

8.1.3 Shielding

Physical barriers such as lead walls, rolling lead screens, and shielded syringes serve to attenuate radiation exposure. Fixed facilities like imaging suites and patient rooms should be designed with adequate wall and window shielding as per regulatory requirements. For mobile work, use portable lead shields and ensure staff wear personal protective equipment when appropriate.

Table 8.1: Specific hazards of common therapeutic radiopharmaceuticals.

Radiopharmaceutical	Type of Emission	Example Use	Radiation Protection Concerns
Iodine-131	• Beta (Mean Energy 196 kev) • Gamma energy (364 keV)	• Thyroid cancer treatment	• High external dose • contamination from urine/sweat • requires room isolation
Lutetium-177	• Beta (Mean Energy 133 kev) • Gamma energy (208 keV)	• Neuroendocrine tumors, prostate cancer	• Lower gamma dose but prolonged exposure from delayed clearance
Yttrium-90	• Pure beta emitter (Mean Energy 935 kev)	• Liver radioembolization (SIRT)	• Bremsstrahlung radiation • requires shielding • minimal contamination risk

8.2 Work Practices in Dosimetry

8.2.1 Patient Interaction

Patient interaction involves tasks requiring direct patient contact such as imaging, urine or blood sampling. Staff must minimize time spent near the patient, standing as close as strictly necessary, and whenever possible, remain behind shielding. Biological samples should be collected using non-contact techniques to reduce direct exposure, and strict hygiene measures must be maintained to prevent the spread of radionuclide contamination.

8.2.2 Imaging and Sampling

Dosimetric procedures such as whole-body scans, SPECT/CT imaging, and blood sampling require balancing accuracy with staff safety. To minimize radiation exposure, personnel should operate imaging equipment using remote controls whenever possible. Leaded glass barriers must be positioned between staff and patients to enhance protection. At the same time, staff must ensure that patient

positioning and image acquisition are performed accurately and efficiently, adhering to the ALARA principle by reducing exposure time and maintaining appropriate shielding and distance.

8.3 Use of Personal Dosimetry

Monitoring personal radiation exposure is essential. Whole-body dosimeter badges should be worn at chest-level, outside any lead aprons, to accurately monitor dose to the torso, including vital organs. When handling patients or radiopharmaceuticals with hands near radiation sources, extremity dosimeters such as ring badges must be worn on the hand most likely to be exposed, typically beneath gloves. Dosimeter readings should be exchanged and processed monthly or as required by local regulations to ensure continuous monitoring. Dose records must then be regularly reviewed to verify that exposure remains within acceptable limits. In cases where any staff member exceeds action levels, an investigation must be initiated promptly, and procedural changes implemented as necessary to enhance safety and compliance.

8.4 Controll Areas and Patient Wards

Patients undergoing therapy with high-activity MRT, such as I-131 or Lu-177, are typically accommodated in a dedicated isolation ward that meets all radiation protection requirements. This controlled area must restrict access to authorized personnel only, display radiation warning signage, and feature structural shielding in walls and doors to protect adjacent spaces. The ward should also include dedicated sanitary facilities to prevent cross-contamination. Depending on national regulations and the activity level administered, admission to such a shielded isolation ward may be mandatory.

8.5 Handling Contamination and Waste

The management of radioactive contamination and waste is a critical component of radiation safety in nuclear medicine practice. Proper handling minimizes radiation exposure to staff, patients, and the environment while ensuring compliance with national and international safety regulations

8.5.1 Contamination Risk

Therapeutic radiopharmaceuticals may be excreted via urine, saliva, sweat, or faeces, presenting a real risk of contamination. To minimize exposure, staff must wear disposable gloves and lab coats when handling potentially contaminated materials and avoid taking these items into clean or unrestricted areas. Floors and patient beds should be protected using absorbent materials, such as pads or

sheets, to trap spills. All reusable instruments must be surveyed for contamination before reuse to ensure safety protocols are upheld.

8.5.2 Waste Management

Radionuclide waste must be managed with caution, using designated shielded and clearly labelled containers. Practices should include:

1) Short-lived radionuclides, typically those with physical half-lives of up to about 10 days, or with measured dose rates less than twice the ambient background or below 5 μSv h^{-1}, may be safely disposed of as general waste once these conditions are verified and documented.

2) Isotopes with longer half-lives or those contaminated with long-lived radionuclides must be returned to a licensed supplier or sent for authorized disposal especially when decay in storage is not feasible.

All waste management practices must comply with pertinent local radiation safety and environmental regulations, with strict labelling, secure storage, and full traceability throughout the process.

8.6 Patient Education and Cooperation

Staff should educate patients to minimize their contribution to radiation exposure:

1) Maintain distance from staff, family, and visitors.

2) Use designated bathrooms and flush twice after use.

3) Practice good hygiene, especially handwashing.

4) Report spills or accidents immediately to staff.

Patient compliance improves safety for everyone involved and ensures accurate data collection for dosimetry.

8.7 Emergency Preparedness

In the event of an accidental spill, patient fall, or equipment failure involving radiopharmaceuticals, non-essential personnel must be evacuated immediately and the affected area secured to prevent further access. The contamination zone should be clearly isolated and marked, using absorbents or appropriate barriers to contain any spread, and contamination monitors deployed to assess radiation levels throughout. Once the scene is secure, the Radiation Protection Officer (or

Medical Physicist) should be contacted without delay to guide decontamination procedures following protocols.

Finally, the incident must be documented and reported in accordance with hospital policy, ensuring full accountability and the opportunity for procedural review and improvement.

8.8 Staff Training and Continuous Education

All personnel involved in nuclear medicine dosimetry must complete comprehensive initial training in radiation safety and participate in regular refresher courses typically on an annual basis or as dictated by regulatory requirements. Hands-on workshops should be included to ensure proficiency in equipment operation, spill management procedures, and other critical tasks. Emergency drills, especially those simulating contamination or exposure incidents, must also be conducted routinely to reinforce preparedness.

Moreover, training participation must be meticulously recorded, and staff competency evaluated regularly to maintain high standards in safety and performance. Consistent documentation of these educational activities ensures compliance and supports ongoing quality assurance.

8.9 Regulatory Limits and Monitoring

According to the International Commission on Radiological Protection (ICRP) and typical national radiation safety regulations, occupational dose limits are generally set at an average of 20 mSv per year over a rolling five-year period, with a maximum of 50 mSv in any single year. Equivalent dose limits for specific body parts may be significantly higher: the skin, hands, and feet may receive up to 500 mSv per year. After pregnancy is declared, the additional dose to the embryo or fetus must remain below 1 mSv for the rest of the pregnancy, and pregnant workers are therefore typically excluded from duties involving therapeutic nuclear medicine.

Monitoring occupational dose records is critical. These records should be reviewed regularly, and any instance of dose limit exceedance must trigger an immediate investigation and implementation of corrective actions to ensure safety and regulatory compliance.

Staff working in nuclear medicine dosimetry are at increased risk of radiation exposure, particularly when handling patients who have received high-activity therapeutic radiopharmaceuticals. By adhering to the principles of time, distance, and shielding and incorporating robust protocols for contamination

control, patient management, and waste disposal staff can maintain a safe working environment.

Ongoing education, dose monitoring, and procedural audits help ensure the safety and health of all involved personnel, aligning with national regulations and best practices in radiation protection.

8.10 References

Hindorf, C., Glatting, G., Chiesa, C., Linden, O., Flux, G., & EANM Dosimetry Committee. (2021). EANM Dosimetry Committee guidelines for dosimetry reporting in therapy using radiopharmaceuticals. *European Journal of Nuclear Medicine and Molecular Imaging, 48*(12), 4371–4385.

International Atomic Energy Agency (IAEA). (2018). *Radiation protection and safety in medical uses of ionizing radiation* (Safety Standards Series No. SSG-46). IAEA.

International Commission on Radiological Protection (ICRP). (2007). *The 2007 recommendations of the International Commission on Radiological Protection* (ICRP Publication 103). *Annals of the ICRP, 37*(2–4).

National Council on Radiation Protection and Measurements (NCRP). (2006). *Management of radionuclide therapy patients* (NCRP Report No. 155). NCRP.

U.S. Nuclear Regulatory Commission (US NRC). (2020). *10 CFR Part 20 – Standards for protection against radiation.* U.S. Government Printing Office.

SUMMARY

The *Handbook of Internal Dosimetry in Nuclear Medicine (2026)* provides guidance on calculating radiation doses from radiopharmaceuticals used in diagnosis and therapy. It focuses on patient-specific dosimetry using methods like the MIRD schema, supported by imaging (SPECT, PET) and tools such as OLINDA/EXM. This book also explains how radionuclide drugs behave in the body and how to estimate ADs to organs and tumors. It includes practical case studies (e.g. I-131, Lu-177, Y-90) and outlines safety practices for healthcare staff.

The handbook emphasizes the growing importance of patient-specific dosimetry, especially in MRT. Aims to guide medical physicists in standardized methodologies for dose assessment, aligning with ICRP, IAEA, and MIRD standards. It discusses the difference between diagnostic (lower dose, more uniform distribution) and therapeutic (higher, often heterogeneous dose) applications.

Methods used are organ-level dosimetry (OLINDA/EXM) and voxel-based dosimetry (3D S-values, Monte Carlo). These methods have limitations, as they are labor-intensive and require serial imaging along with accurate anatomical segmentation

This handbook presents real dosimetry workflows for I-131 for Differentiated Thyroid Cancer (DTC), PRRT Lu-177 with Pre-MRT scans using I-131 or Tc-99m tracer, Post- MRT dosimetry using Y-90 or Lu-177 include blood and whole-body measurements.

Emphasizes the importance of Personalized internal dosimetry in therapy, Accurate biokinetic modeling and imaging, Protection of patients and staff, encourages consistent use of validated tools and standardized methodologies and recommends continuous education and improvement in internal dosimetry practices

In summary, the handbook provides both theoretical and practical knowledge to support safe, effective, and personalized use of radiopharmaceuticals in nuclear medicine, aligned with international standards and guidelines.

APPENDIX A: PROCEDURE FOR GENERATING Ã USING OLINDA/EXM

a) The main OLINDA/EXM menu interface of the program is shown in Figure 1.

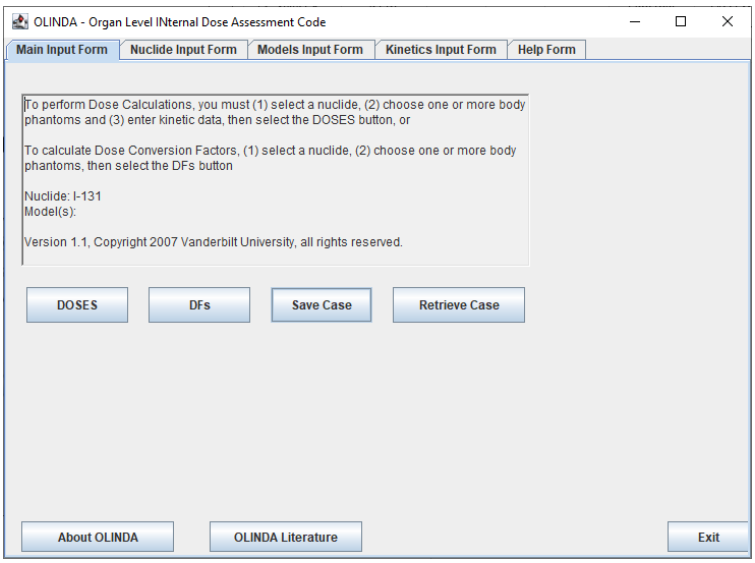

Figure 1: OLINDA/EXM Main Menu Form.

b) Select the radionuclide inside the **Nuclide Input Form** as shown at Figure 2.

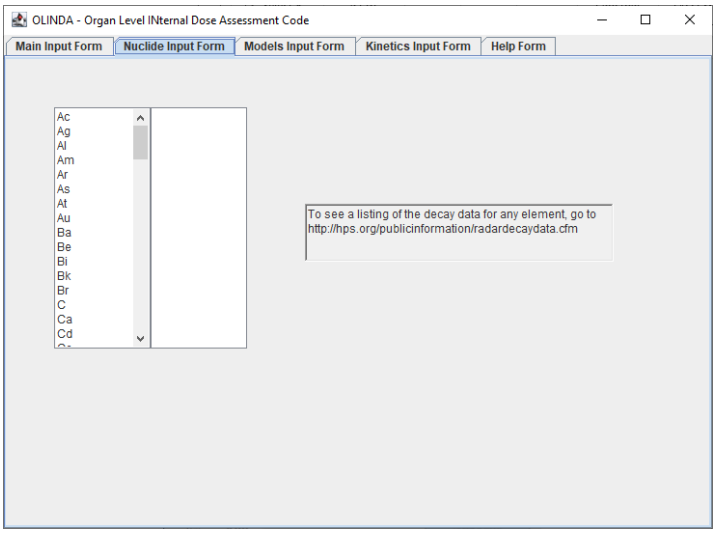

Figure 2: Nuclide Input Form.

c) In the Models Input Form (Figure 3), select the appropriate phantom model (e.g., Adult Male or Adult Female) based on the ORNL standard. For tumor AD estimation, click on the Spheres model to utilize sphere-based dosimetry.

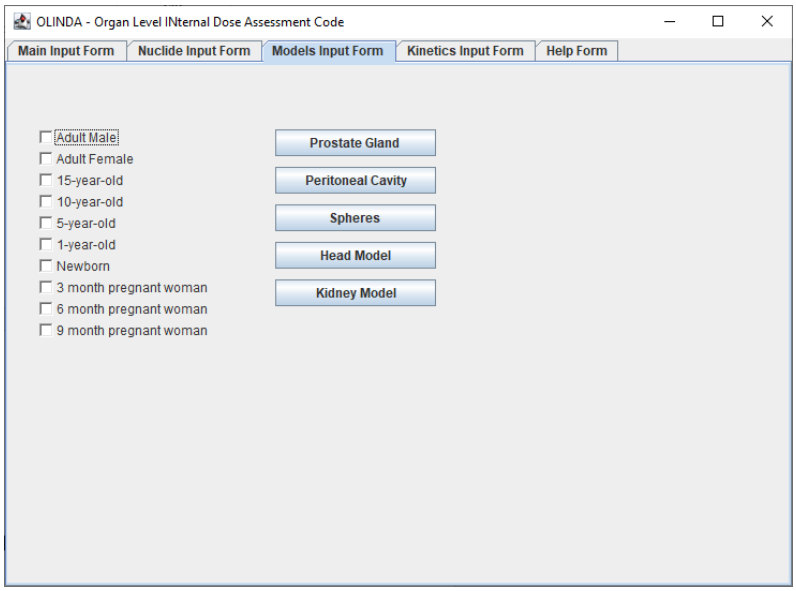

Figure 3: Model Input Form.

d) In the **Kinetics Input Form**, select the **Fit Data to Model** option from the menu, as illustrated in Figure 4.

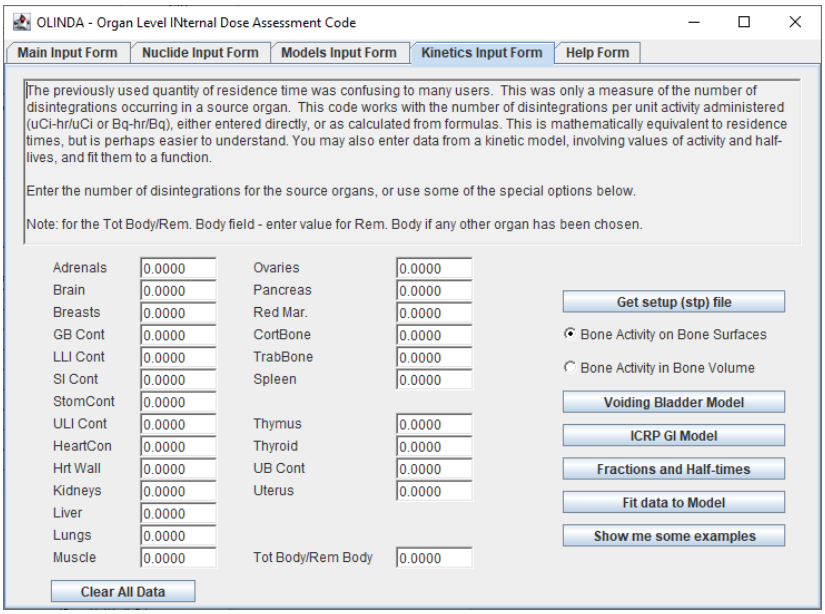

Figure 4: Kinetic Input Form.

e) **Disintegrations Calculator null sheet**: Select the identify organ as shown at **Error! Reference source not found.**.

i. Enter the “Time (h)” and “Observed %ID”

ii. Insert any numerical values or use “-1” as a placeholder in columns A, B, a, and b as required.

1. A represents Initial amplitude (MBq or %IA) of the **fast** component
2. B represents Initial amplitude (MBq or %IA) of the **slow** component
3. c represents decay constant related with **fast** component
4. d represent decay constant related with **slow** component

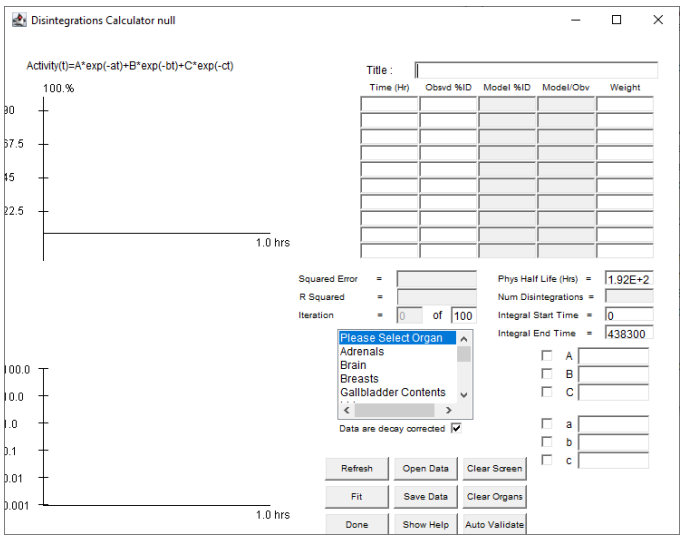

Figure 5: Disintegrations Calculator null sheet.

iii. Click **"Fit"** repeatedly until the R Squared value is close to 1 to estimate the Number of Disintegrations or $\tilde{A}$.

iv. Apply the same procedure to the rest of organ, as illustrated in Figure 5 and Figure 6.

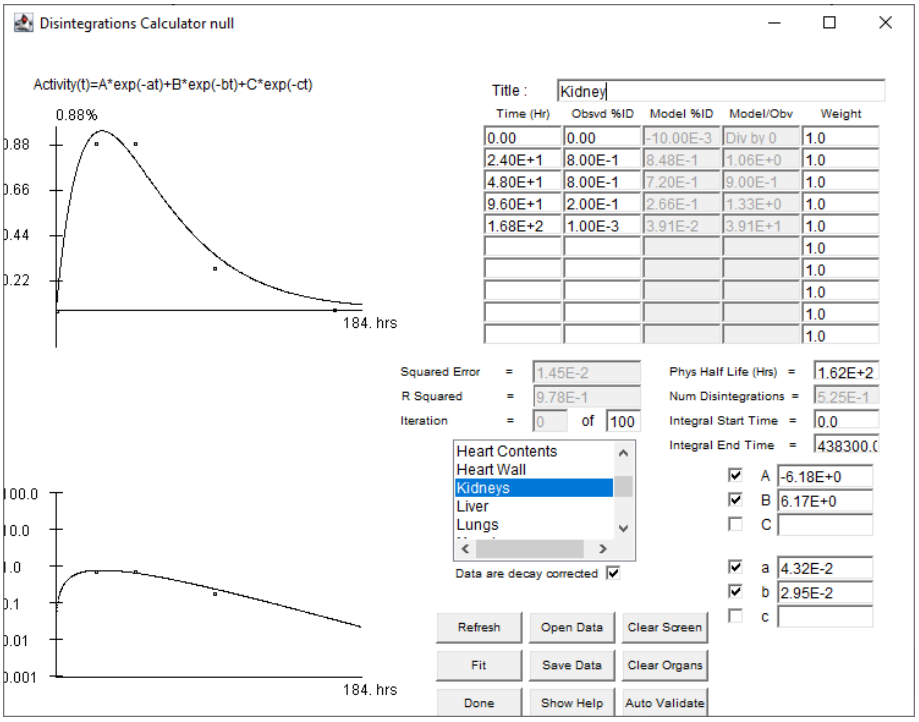

Figure 6: Example of Disintegrations Calculator null sheet for kidneys.

APPENDIX B: PROCEDURE FOR ESTIMATING AD USING OLINDA/EXM

a) In the **Main Input Form**, click on the “DOSES” button to initiate dose calculation Figure 1.

b) In the Nuclide Input Form, select the desired radionuclide, referring to the options listed in Figure 2.

c) In the **Model Input Form**, select the suitable phantom model for organ at risk, and spheres for tumor dosimetry as illustrated in Figure 3.

d) In the **Kinetics Input Form**, ensure that the $\widetilde{A}$ is entered for the relevant OAR or tumor, as illustrated in Figure 4.

e) If the $\widetilde{A}$ is to be derived from raw time-activity curve data, open the *Disintegrations Calculator (null sheet)* and follow the procedure outlined in Step (e) of **APPENDIX A**, as illustrated in Figure 5 and Figure 6.

f) Return to the **Main Input Form** and select the “**DOSES**” button once again to proceed with the dose calculation, as depicted in Figure 1.

g) To ensure accurate organ sizing, note that the default OLINDA phantom uses standard ORNL reference organ masses. For patient-specific customization, click the “**Modify Input Data**” button in the **Modify Input Data** output screen, as shown in Figure 7.

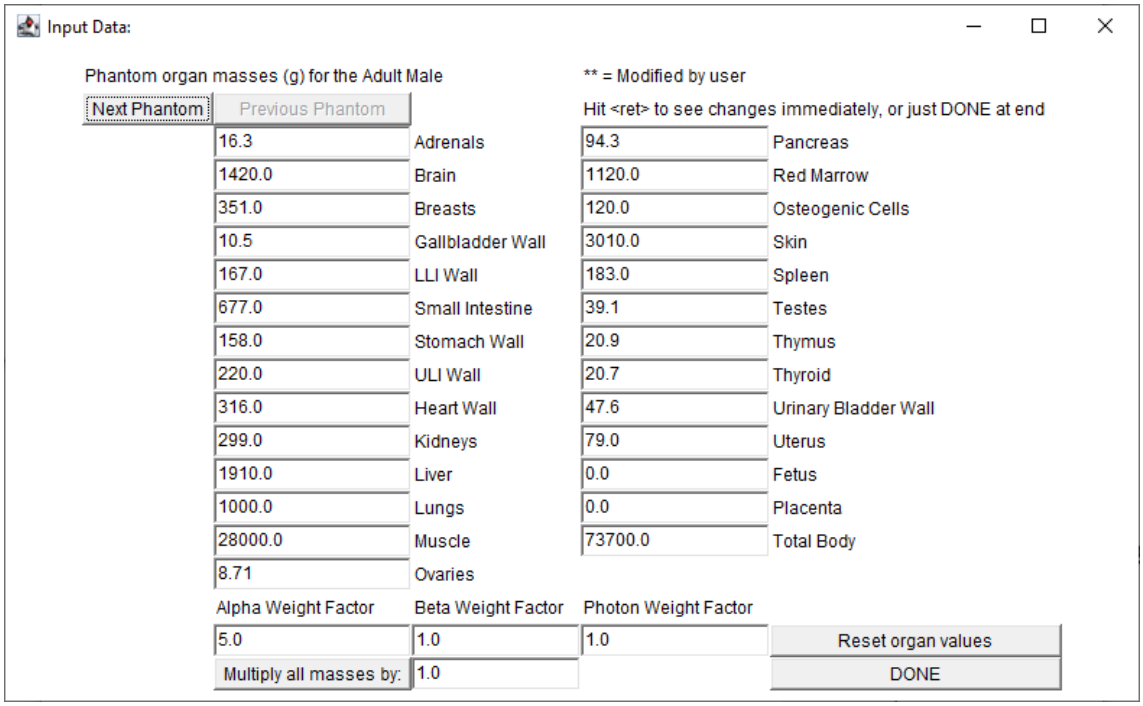

Figure 7: The “Modify Input Data” section allows customization of organ sizes before finalizing calculations.

h) In the Input Data output screen, manually enter the patient-specific organ masses for the relevant organs. After updating all necessary values, click “**Done**” to confirm and apply the changes, as illustrated in Figure 7.

i) In the **Organ Doses** output screen, the software will display the AD for each organ in either mGy MBq^{-1} or Gy GBq^{-1}, based on the modified input data, as shown in Figure 9. To calculate the mean AD, enter the administered activity by click “**Mult. Dose by (MBq)**” button.

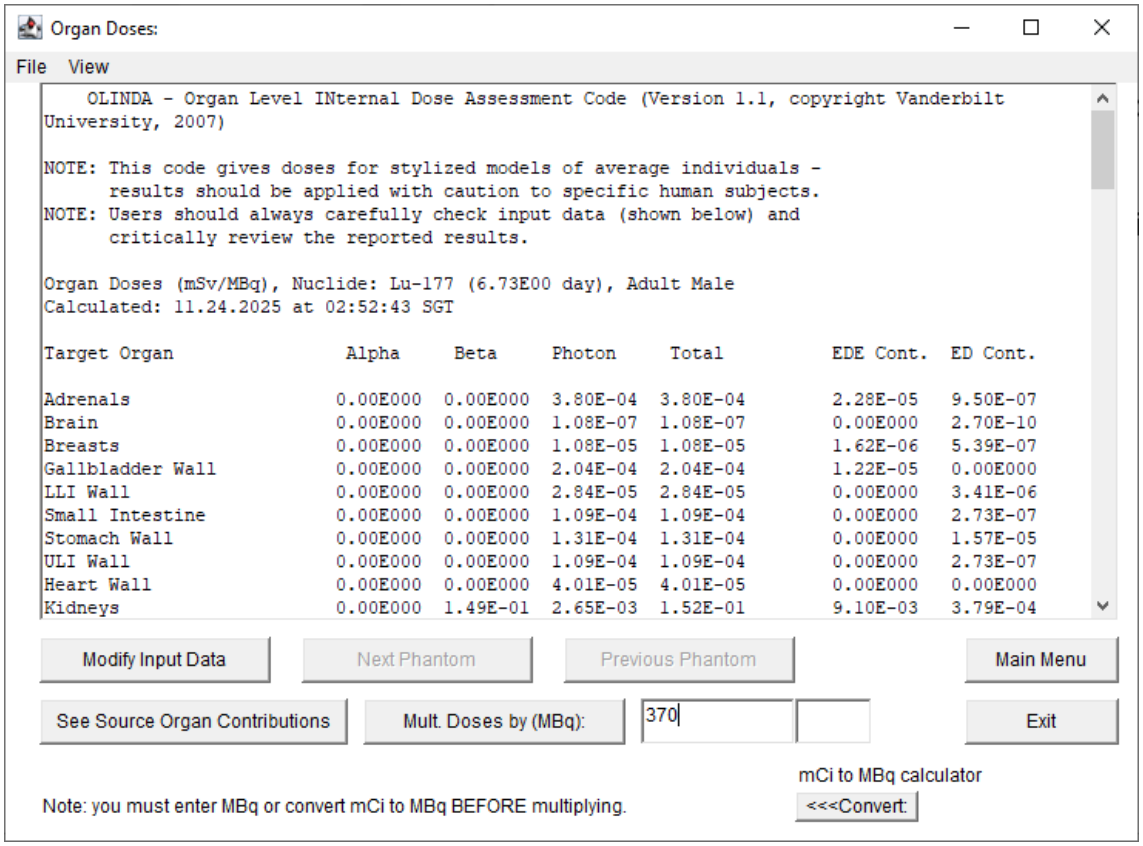

Figure 8: Organ Doses sheet.

j) To estimate the tumor AD, select the Spheres input model, as illustrated in Figure 3.

k) Enter the $\tilde{A}$ obtained from step (v), then click "**Calculate Dose**" to confirm. Use curve fitting to estimate the AD mGy MBq^{-1} based on the tumor mass, as illustrated in Figure 9.

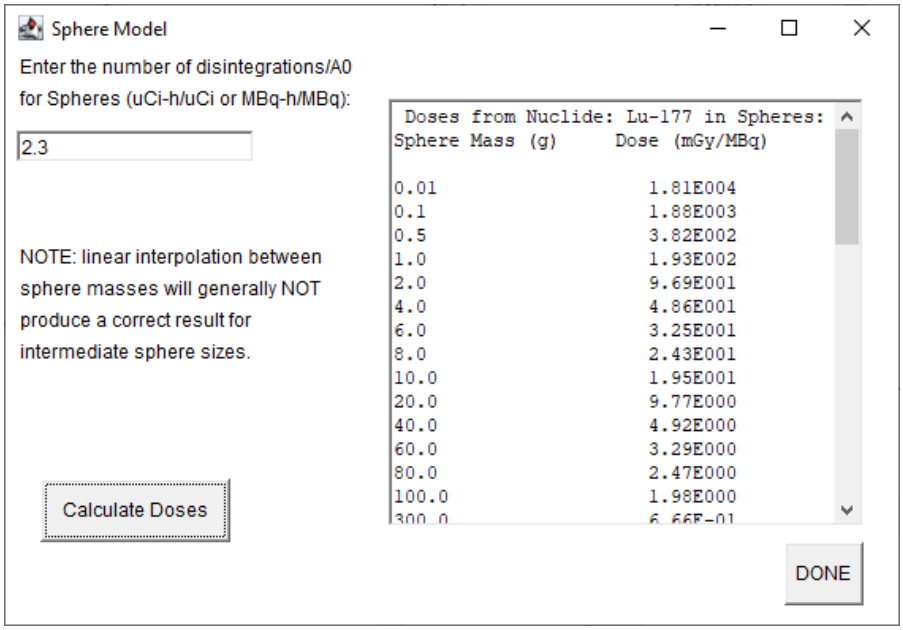

Figure 9: Sphere Model output screen for tumor dosimetry in OLINDA/EXM.

CONTRIBUTORS TO DRAFTING AND REVIEW

Dr. Mohamad Aminudin bin Said (Editor) Tuan Solawati binti Tuan Muda Ummi Habibah binti Ibrahim	Institut Kanser Negara
Haizana binti Hairuman Dr. Nabilah Solehah binti Ahmad Tamrin Muhammad Izzat bin Mohamad Aseri	Hospital Kuala Lumpur
Mohd Hizwan bin Mohd Yahya Dr. Fatin Nadhirah binti A Halim Dr. Prema Devi Chellayah	Hospital Pulau Pinang
Dr. Mohd Akmal bin Masud	Hospital Umum Sarawak
Nurul Diyana binti Shariff Norhazlina binti Hassan	Hospital Sultanah Aminah

SECRETARIATS

Mohd Khairudin bin Mohamed Samsi Dr. Soh Hwee Shin Nur Alia Fauzia binti Abdullah Dr. Faezeah binti Abd Ghani	Medical Radiation Surveillance Division

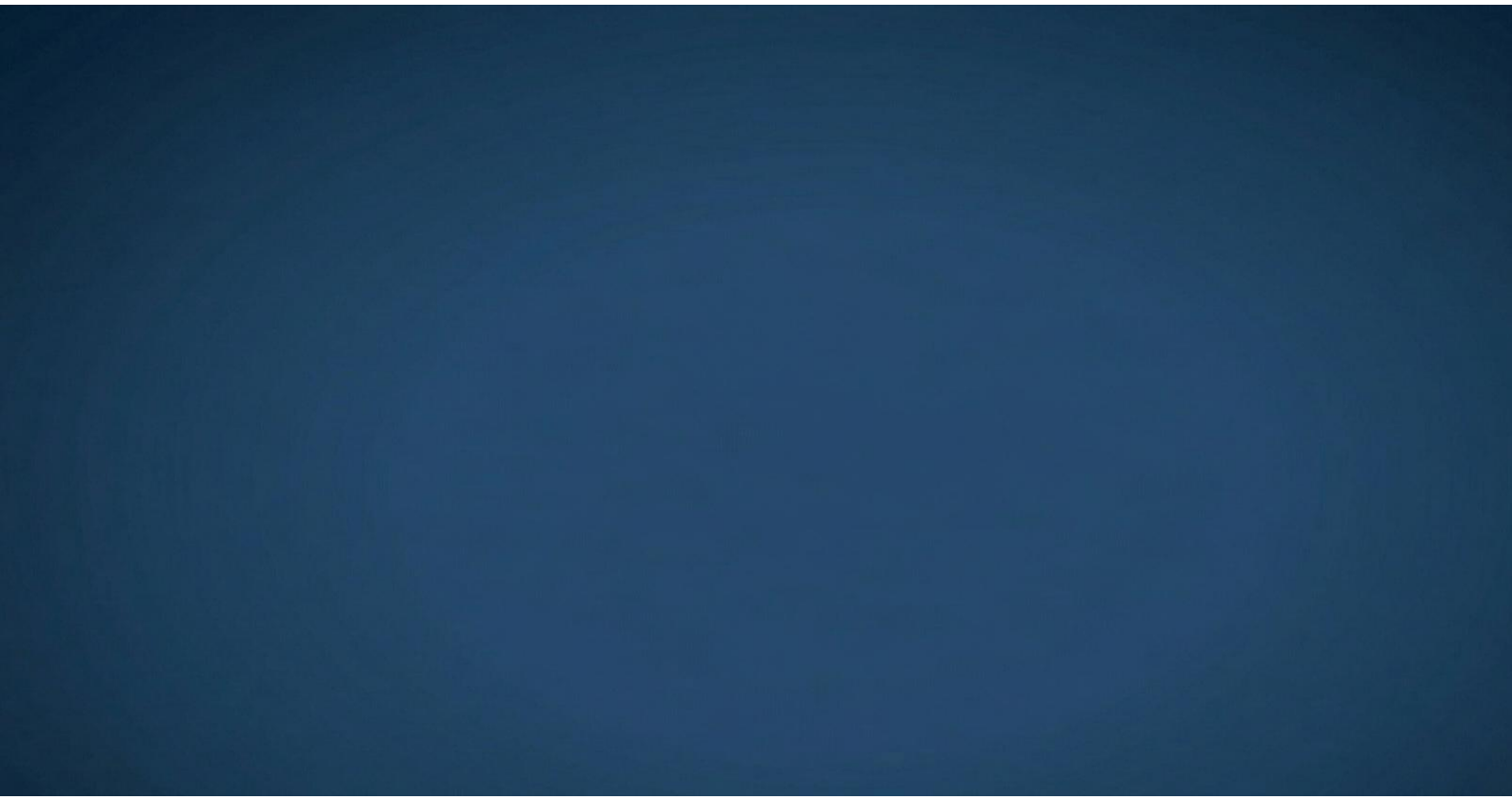

eISBN 978-967-2469-87-2

MINISTRY OF HEALTH
MEDICAL RADIATION SURVEILLANCE DIVISION